

WATER DISPERSIBLE α -MANGOSTIN BY SELF-ASSEMBLY PROCESS



A Thesis Submitted in Partial Fulfillment of the Requirements

for the Degree of Master of Science in Chemistry

Department of Chemistry

Faculty of Science

Chulalongkorn University

Academic Year 2019

Copyright of Chulalongkorn University

แอลฟาแมงโกสตินที่กระจายตัวได้ในน้ำจากกระบวนการจัดตัวเอง



วิทยานิพนธ์นี้เป็นส่วนหนึ่งของการศึกษาตามหลักสูตรปริญญาวิทยาศาสตรมหาบัณฑิต

สาขาวิชาเคมี ภาควิชาเคมี

คณะวิทยาศาสตร์ จุฬาลงกรณ์มหาวิทยาลัย

ปีการศึกษา 2562

ลิขสิทธิ์ของจุฬาลงกรณ์มหาวิทยาลัย

Thesis Title WATER DISPERSIBLE α -MANGOSTIN BY SELF-
ASSEMBLY PROCESS

By Miss Jutamad Bumrung

Field of Study Chemistry

Thesis Advisor Professor Supason Wanichwecharunguang, Ph.D.

Accepted by the Faculty of Science, Chulalongkorn University in Partial
Fulfillment of the Requirement for the Master of Science

..... Dean of the Faculty of Science
(Professor POLKIT SANGVANICH, Ph.D.)

THESIS COMMITTEE

..... Chairman
(Associate Professor VUDHICHAJ PARASUK, Ph.D.)

..... Thesis Advisor
(Professor Supason Wanichwecharunguang, Ph.D.)

..... Examiner
(Associate Professor Voravee Hoven, Ph.D.)

..... External Examiner
(Varol Intasanta, Ph.D.)

จุฬามาศ บำรุง : แอลฟาแมงโกสตินที่กระจายตัวได้ในน้ำจากกระบวนการจัดตัวเอง . (WATER DISPERSIBLE α -MANGOSTIN BY SELF-ASSEMBLY PROCESS) อ.ที่ปรึกษาหลัก : ศ. ดร. ศุภศร วนิชเวชรุ่งเรือง

แอลฟาแมงโกสตินเป็นสารออกฤทธิ์ทางชีวภาพสำคัญที่พบมากในสารสกัดจากเปลือกมังคุด (*Garcinia mangostana* Linn) แอลฟาแมงโกสตินมีฤทธิ์ทางชีวภาพที่หลากหลายแต่มีความสามารถในการละลายน้ำต่ำ ทำให้มีข้อจำกัดในการนำไปประยุกต์ใช้งานกับเครื่องสำอางค์และยา ในงานวิจัยนี้ผู้วิจัยจึงแก้ไขปัญหาดังกล่าวโดยการสร้างอนุภาคแอลฟาแมงโกสตินที่กระจายตัวได้ในน้ำจากกระบวนการจัดตัวเอง โดยไม่จำเป็นต้องใช้พอลิเมอร์หรือสารลดแรงตึงผิวในกระบวนการ กระบวนการจัดตัวเองดังกล่าวเป็นกระบวนการที่ทำได้ง่าย และให้อนุภาคทรงกลมระดับนาโนเมตรที่ประกอบด้วยแอลฟาแมงโกสติน 100% ข้อมูลจากเทคนิค FT-IR แสดงให้เห็นว่าแรงระหว่างโมเลกุลที่เกิดขึ้นในการก่อตัวอนุภาคนาโนแมงโกสติน แข็งแรงน้อยกว่าแอลฟาแมงโกสตินที่เป็นสารตั้งต้น ซึ่งสอดคล้องกับเสถียรภาพทางความร้อนที่ลดลงเมื่อแอลฟาแมงโกสตินก่อตัวเป็นอนุภาค ข้อมูลจากเทคนิค XPS แสดงให้เห็นว่ามีการสะสมของหมู่ฟังก์ชันที่มีซัลเฟอร์ที่บริเวณพื้นผิวของอนุภาคมากขึ้นกว่าแอลฟาแมงโกสตินดั้งเดิม แต่เมื่ออนุภาคของแอลฟาแมงโกสตินอยู่ในรูปของสารละลายยังคงมีโครงสร้างทางเคมีเหมือนกับสารตั้งต้น นอกจากนี้ในงานวิจัยนี้ได้สังเคราะห์อนุพันธ์ของแอลฟาแมงโกสตินโดยการแทนที่หมู่ไฮดรอกซิลด้วยหมู่บิลทิว และใช้อนุพันธ์ดังกล่าวสร้างอนุภาคที่กระจายตัวได้ในน้ำด้วยวิธีการเดียวกับการเตรียมอนุภาคนาโนแมงโกสติน ซึ่งพบว่าไม่สามารถสร้างอนุภาคที่กระจายตัวได้ในน้ำจากอนุพันธ์ที่ไม่มีหมู่ไฮดรอกซิลได้ ผลดังกล่าวช่วยยืนยันว่าหมู่ไฮดรอกซิลเป็นส่วนสำคัญที่ทำให้แอลฟาแมงโกสตินก่อตัวเป็นอนุภาคทรงกลม เมื่อทำการทดสอบฤทธิ์ทางชีวภาพในการยับยั้งเชื้อแบคทีเรียที่เป็นสาเหตุของการเกิดสิวของอนุภาคนาโนแมงโกสตินที่ได้ พบว่าอนุภาคนาโนแมงโกสตินยังคงมีฤทธิ์การยับยั้งเชื้อสิวใกล้เคียงกับแอลฟาแมงโกสตินที่เป็นสารตั้งต้น และเมื่อทำการทดสอบฤทธิ์ทางชีวภาพในการต้านการอักเสบของอนุภาค พบว่าที่ความเข้มข้น 12.7 ส่วนในล้านส่วน ซึ่งเป็นความเข้มข้นที่ไม่เป็นพิษต่อเซลล์ อนุภาคนาโนแมงโกสตินมีฤทธิ์ในการต้านการอักเสบสูงกว่าแอลฟาแมงโกสตินที่เป็นสารตั้งต้นถึง 5 เท่า

สาขาวิชา เคมี
ปีการศึกษา 2562

ลายมือชื่อนิสิต
ลายมือชื่อ อ.ที่ปรึกษาหลัก

6072036123 : MAJOR CHEMISTRY

KEYWORD: α -mangostin, self-assembly process, water dispersible particles, α -mangostin nanoparticles

Jutamad Bumrung : WATER DISPERSIBLE α -MANGOSTIN BY SELF-ASSEMBLY PROCESS. Advisor: Prof. Supason Wanichwecharungruang, Ph.D.

α -Mangostin, major bioactive compounds in *Garcinia mangostana* Linn, displays various interesting biological activities. However, the poor water solubility of α -mangostin has limited its use in the cosmetics and pharmaceuticals. Here, we solve α -mangostin's solubility by creating water dispersible α -mangostin particles through self-assembly process with no need of any auxiliary agents such as polymers or surfactants. The simple and upscalable process gives 100% pure α -mangostin spherical particles with nanometer sizes. FT-IR result suggests that intermolecular interaction among α -mangostin molecules in the nanoparticles is weaker than that of the original α -mangostin solid. The lower thermal stability of the particles as compared to that of the original α -mangostin agree with the FT-IR result. The XPS results of α -mangostin particles show more accumulation of hydrophilic functional groups at the surface than that observed at the surface of the original α -mangostin. Nevertheless, the obtained water dispersible α -mangostin particles show the same chemical structure as the original α -mangostin. 3,6-Dibutoxy- α -mangostin prepared through the S_N2 substitution reaction, could not form water dispersible particles using similar preparation process. This helps strengthening our hypothesis that the hydroxyl group of α -mangostin molecules is essential for the water-dispersibility character of the self-assembled particles. The water dispersible α -mangostin particles show a similar anti-acne activity to that of the original α -mangostin. At 12.7 ppm (non-cytotoxic concentration), the anti-inflammatory activity of α -mangostin nanoparticles is 5 times higher than that of the original α -mangostin.

Field of Study: Chemistry

Student's Signature

Academic Year: 2019

Advisor's Signature

ACKNOWLEDGEMENTS

I would first like to thank my advisor, Professor Dr. Supason Wanichwecharungruang for her generous assistance and providing me insight and expertise that greatly supported this research. I gratefully acknowledge the committees, Associate Professor Dr. Vudhichai Parasuk, Associate Professor Dr. Voravee Hoven and Dr. Varol Intasanta for their time, comment, and suggestions on my work. I also gratefully appreciate to Associate Professor Dr. Tanapat Palaga for guidance and helps in anti-inflammatory test and Associate Professor Dr. Chanpen Chanchao for suggestion and helps in the anti-acne test. Also, I thank members of the SW research group and all of my friends for their friendships and any helps. I would like to thank my gratitude to the Department of Chemistry, Faculty of Science, Chulalongkorn University. Last but not least, I would like to thank my family for their support.

Jutamad Bumrung

TABLE OF CONTENTS

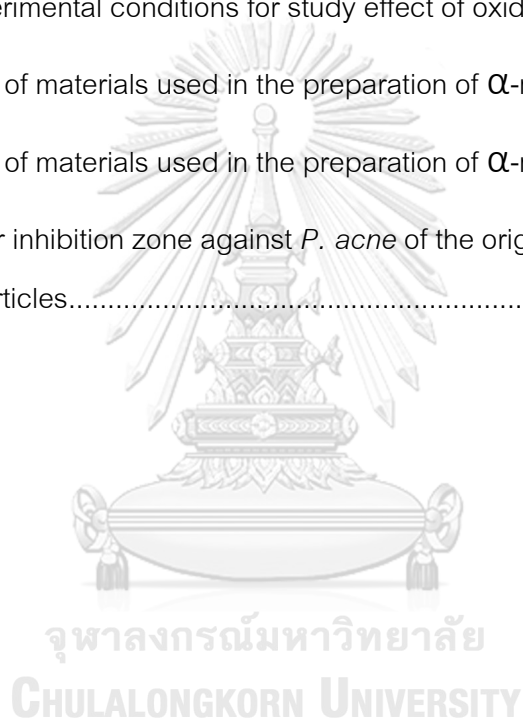
	Page
ABSTRACT (THAI)	iii
ABSTRACT (ENGLISH)	iv
ACKNOWLEDGEMENTS	v
TABLE OF CONTENTS	vi
LIST OF TABLES	ix
LIST OF FIGURES	x
CHAPTER I INTRODUCTION	1
1.1 α -Mangostin	1
1.2 Literature review anti-inflammatory activity of α -mangostin	4
1.3 Literature review anti-acne activity of α -mangostin	6
1.4 Objective and scope of work	7
CHAPTER II EXPERIMENTAL	8
2.1 Materials and Chemicals	8
2.1.1 Media culture and chemical reagent for cell culture and treatment	8
2.1.2 Media culture for anti-acne study	9
2.2 Instruments and Equipment	9
2.3 Optimization process for preparing of water dispersible α -mangostin	10
2.3.1 Preparation of phosphate buffer	10
2.3.2 Preparation of water dispersible α -mangostin through enzymatic template polymerization	10
2.3.2.1 Effect of enzyme	10

2.3.2.2 Effect of polymer	11
2.3.2.3 Effect of oxidizing agent.....	12
2.4 Self-assembly of α -mangostin	12
2.4.1 Preparation of water dispersible α -mangostin particles through self-assembly process.....	12
2.4.1.1 Effect of α -mangostin concentration used	13
2.4.1.2 Effect of ethanol ratio	14
2.4.1.3 Effect of the type of organic solvent used for dissolving α -mangostin	14
2.5 Self-assembly of α -mangostin derivative	15
2.5.1 Synthesis of α -mangostin derivative.....	15
2.5.2 Preparation of α -mangostin derivative (dMG) through self-assembly process	16
2.6 Anti-inflammatory activity and cell viability	16
2.6.1 Preparation of complete media	17
2.6.2 Preparation of tested sample	17
2.6.3 Preparation of Nitrite standards for standard curve	17
2.6.4 Cell culture conditions and cell treatment.....	17
2.6.5 Determination of nitric oxide production using nitric oxide assay.....	18
2.6.6 Determination of cell viability using MTT assay.....	18
2.7 Anti-acne activity	19
2.7.1 Preparation of brain heart infusion broth.....	19
2.7.2 Preparation of brain heart infusion agar base	19
2.7.3 Preparation of tested sample	20

2.7.4 Bacterial culture and treatment.....	20
CHAPTER III RESULTS AND DISCUSSIONS.....	22
3.1 Optimizing the preparation of water dispersible α -mangostin.....	22
3.2 Self-assembly of α -mangostin	26
3.2.1 Chemical structure of α -mangostin nanoparticles.....	30
3.2.2 Photophysical property of α -mangostin nanoparticles.....	32
3.2.4 Particle size and zeta potential	35
3.2.5 Crystallinity of α -mangostin nanoparticles.....	36
3.2.6 Thermal stability of α -mangostin nanoparticles.....	37
3.2.7 Functional groups at the surface of the particles	38
3.2.8 The phenomenon of α -mangostin nanoparticle formation.....	40
3.3 Self-assembly of α -mangostin derivative.....	42
3.4 Anti-inflammatory activity and cell viability	44
3.5 Anti-acne activity	45
CHAPTER IV CONCLUSION.....	47
REFERENCES.....	49
APPENDIX.....	52
VITA	58

LIST OF TABLES

Table 1.1 In vitro cytotoxicity activity (IC_{50} , μM) of cancer cell lines of α -mangostin analogs modified.	2
Table 2.1 The experimental conditions for study effect of enzyme.	11
Table 2.2 The experimental conditions for study effect of polymer.	11
Table 2.3 The experimental conditions for study effect of oxidizing agent.	12
Table 2.4 Amounts of materials used in the preparation of α -mangostin particles.	13
Table 2.5 Amounts of materials used in the preparation of α -mangostin particles.	14
Table 3.1 The clear inhibition zone against <i>P. acne</i> of the original α -mangostin solid and nanomangostin particles.	46



LIST OF FIGURES

Figure 1.1 The structure of α -mangostin analogs modified.	2
Figure 1.2 Nitrite production from LPS-stimulated RAW 264.7 cells co-treated with α - or γ -mangostin.....	5
Figure 3.1 SEM images of enzymatic template polymerization products obtained at the amounts of HRP of (a) 0x; (b) 0.003x; (c) 0.006x; (d) 0.012x; (e) 0.030x and (f) 0.045x of α -mangostin.....	24
Figure 3.2 SEM images of enzymatic template polymerization products obtained at the molecular weights of PEG of (a) 0; (b) 200; (c) 400; (d) 600; (e) 950; (f) 2050 and (g) 35000 g/mol.....	25
Figure 3.3 SEM images of enzymatic template polymerization products obtained at the amounts of H ₂ O ₂ of (a) 0; (b) 6; (c) 8; (d) 10 and (e) 15 % v/v.....	25
Figure 3.4 NMR spectra of the original α -mangostin solid, enzymatic template polymerization products (pMG) obtained at the molecular weight of PEG at 35,000 g/mol, HRP enzyme at 0.25 mg and H ₂ O ₂ at 6% v/v, and PEG35,000 in CDCl ₃ ,	26
Figure 3.5 SEM images of α -mangostin nanoparticles obtained when using α -mangostin concentration at (a) 0.5; (b) 1.0; (c) 5.0; (d) 10.0 and (e) 30.0% w/v.....	28
Figure 3.6 SEM images of α -mangostin nanoparticles obtained when using amount of ethanol at (a) 0.5; (b) 5.0; (c) 20.0 and (d) 50.0% v/v.....	29
Figure 3.7 SEM images of α -mangostin nanoparticles obtained when using (a) dimethyl sulfoxide; (b) methanol; (c) propanol; (d) butanol and (e) acetone as the organic solvent for dissolving α -mangostin replace ethanol.....	29
Figure 3.8 NMR spectra of the original α -mangostin solid, nMG-E, nMG-P and nMG-B in DMSO-d ₆	31

Figure 3.9 Solid-state ^1H NMR spectra of the original α -mangostin solid and nMG-E...	32
Figure 3.10 UV-Visible spectra of α -mangostin, nMG-E, nMG-P and nMG-B.....	33
Figure 3.11 IR spectra of the original α -mangostin, nMG-E, nMG-P and nMG-B.	34
Figure 3.12 Size distribution in water of (a) nMG-E (b) nMG-P and (d) nMG-B.....	35
Figure 3.13 X-ray diffraction patterns of the original α -mangostin solid, nMG-E, nMG-P and nMG-B.	36
Figure 3.14 Thermograms of the original α -mangostin solid (blue line); nMG-E (red line); nMG-P (green line) and nMG-B (yellow line).....	37
Figure 3.15 XPS results on carbon 1s binding energy of (a) original α -mangostin solid (b) nMG-E (c) nMG-P and (d) nMG-B.....	39
Figure 3.16 The propose schematic represent the phenomenon of α -mangostin nanoparticle formation.	41
Figure 3.17 NMR spectra of the original α -mangostin solid, dMG and bromobutane... ..	43
Figure 3.18 SEM images of (a) dMG and (b) the obtained product from self-assembly process of dMG.	43
Figure 3.19 %NO production in water of the original α -mangostin solid and nMG-E. ...	45
Figure 3.20 %Cell viability in water of the original α -mangostin solid and nMG-E.....	45

CHAPTER I

INTRODUCTION

1.1 α -Mangostin

α -Mangostin or 1,3,6-trihydroxy-7-methoxy-2,8-bis(3-methylbut-2-enyl) xanthen-9-one ($C_{24}H_{26}O_6$) is the major bioactive compounds from *Garcinia mangostana* Linn [1]. α -mangostin had been reported to display various interesting biological activities and pharmacological activities including anticancer [2], anti-inflammatory [3], anti-acne [4], antioxidant [5], antibacterial [6], antifungal [7], antiviral [8], anti-allergy [9] and antimycobacterial activities [10]. However, the aqueous solubility of α -mangostin is 2.03×10^{-4} mg/L at 25°C [11]. This poor water solubility causes low bioavailability of the material. Moreover, the low solubility in water of α -mangostin has limited its uses in the cosmetics and pharmaceutical industries. Organic solvents such as alcohol are used to dissolve α -mangostin for cosmetics and pharmaceutical application. High dose of alcohol is well known to cause skin dryness, skin allergy and skin irritation [12].

Currently, there are several methods to improve the water solubility of α -mangostin. In 2014, Fei *et al.* [13] synthesized the α -mangostin derivatives through the modification of various hydroxyl groups of α -mangostin (Table 1.1) to improve anti-cancer activity. After modification the hydroxyl groups of α -mangostin, the results (Table 1.1) reveal the increased kinetic solubility in 5%DMSO in water of α -mangostin from 20 ± 0.9

to $381 \pm 7 \mu\text{M}$. However, the evaluated anti-cancer activity using 5 human cancer cell lines showed reduced anti-cancer activity.

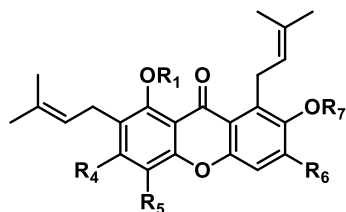


Figure 1.1 The structure of α -mangostin analogs modified.

Table 1.1 In vitro cytotoxicity activity (IC_{50} , μM) of cancer cell lines of α -mangostin analogs modified.

Compound	R1	R4	R5	R6	R7	Solubility (μM)	IC_{50} ($\mu\text{g/L}$)				
							NCI-H460	SW-620	AsPC-1	MDA-MB-231	B16F10
α -mangostin	H	OH	H	OH	CH_3	20 ± 0.9	3.23	2.97	4.02	3.04	3.23
3	H	OH	H	OH	H	94 ± 3	4.48	5.69	5.92	5.87	-
4a	H	OH	H	OCOCH_3	CH_3	148 ± 5	12.63	10.91	13.9	12.9	13.06
4b	H	OCOCH_3	H	OCOCH_3	CH_3	122 ± 2	12.49	22.73	14.25	17.45	15.08
6a	H	OH	H	O-Allyl	CH_3	149 ± 2	12.21	12.13	21.33	17.88	16.52
9	CH_3	OH	H	OH	CH_3	104 ± 4	10.82	18.17	13.9	20.78	16.6
11	H	H	H	NH_2	CH_3	138 ± 6	17.59	15.88	31.34	30.9	14.38
13	H	OH	H	OH	CH_3	78 ± 2	4.17	6.42	4.64	4.91	6.54
14	H	OH	NO_2	OH	CH_3	339 ± 5	16.83	22.61	31.77	28.96	-
16	H	OH	Cl	OH	CH_3	381 ± 7	9.96	9.59	19.26	10.11	12.44

In 2012, Aisha *et al.* [11] improved solubility of α -mangostin through self-assembly of α -mangostin with polyvinylpyrrolidone (PVP) into nanomicelles. The obtained nanomicelles showed particle size in the range of 99-127 nm. These particles can enhance the solubility of α -mangostin from $0.2 \pm 0.2 \mu\text{g/mL}$ to $2743 \pm 11 \mu\text{g/mL}$. Moreover,

the enhanced solubility leads to enhanced cellular uptake of nanomicelles via endocytosis and subsequent potent cytotoxicity.

In 2015, Pan-In *et al.* [14] prepared α -mangostin nanoparticle by encapsulation of α -mangostin with a polymer blend of ethyl cellulose and methyl cellulose (1:1), and studied the anti-acne activity of the obtained material. The particles exhibit the spherical morphology with particle size of 300–500 nm and α -mangostin loading content of $41.90 \pm 0.79\%$. The obtained water-dispersible particles exhibited a better anti-acne activity than the original α -mangostin and showed the sustained release of α -mangostin in human synthetic sebum at 37°C.

In 2019, Yang *et al.* [15] prepared α -mangostin nanomicelles using poly (ethylene glycol)-polycaprolactones (MPEG-PCL) for improving anti-melanoma activity. They found the α -mangostin/MPEG-PCL nanomicelles showed a better inhibitory effect on the melanoma cells (A375 and B16 cells) and lower toxicity in the non-tumor cell lines comparing to the free α -mangostin.

The above research demonstrated that synthesis of α -mangostin nanoparticles via surfactant-based micelles and polymeric encapsulation process gave a good water-dispersible particle, the particle size of less than 600 nm which is an appropriate size for skin application [16-18], with presented the biological activity. But, α -mangostin nanoparticles obtained from these process possess drawbacks such as skin irritation from a surfactant, instability of the surfactant based micelles, low loading capacity, presence of the large amount of surfactants and polymers that the body do not want them.

In 2016, Pukfukdee, P. [19] fabricated polymerized EGCG nanoparticles (P-EGCG) via enzymatic template polymerization using a little of polyethylene glycol (PEG) as a polymer template (EGCG: PEG = 15:1). The obtained dry particles could be stably dispersed in water and showed high cytotoxicity to lung cancer with IC_{50} of 5.0 $\mu\text{g/L}$, which is 5 times higher than that of the original EGCG.

With an interesting method from Pukfukdee's research, here we apply this method to prepare water-dispersible α -mangostin particles by optimizing the reaction condition.

1.2 Literature review anti-inflammatory activity of α -mangostin

In 2008, Chen *et al.* [3] studied anti-inflammatory activity of mangostins by determining NO and PGE_2 production. They found that both α - and γ -mangostins can inhibit nitric oxide (NO) and PGE_2 production from lipopolysaccharide (LPS) stimulated RAW 264.7 cells. The IC_{50} values of α - and γ -mangostins on NO production inhibition were 12.4 and 10.1 μM (Figure 1.2), and IC_{50} values of α - and γ -mangostins on PGE_2 production inhibition were 11.08 and 4.5 μM , respectively.

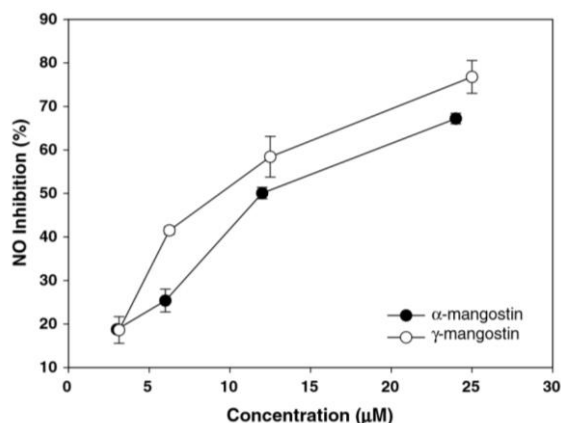


Figure 1.2 Nitrite production from LPS-stimulated RAW 264.7 cells co-treated with α - or γ -mangostin.

In 2009, Bumrungpert *et al.* [20] examined the extent to which α - and γ -mangostins prevented the inflammatory. They found that α - and γ -mangostins prevented inflammation by inhibiting LPS-mediated activation of the JNK, ERK and MAPK p38, and the transcription factors AP-1 and NF- κ B, which is inflammatory genes that cause insulin resistance in human adipocytes.

In 2013, Gutierrez-Orozco *et al.* [21] studied in vitro anti-inflammatory activity of α -mangostin in human cells using interleukin-8 (IL-8) and tumor necrosis factor- α (TNF- α) as biomarker of inflammation. They discovered that anti-inflammatory α -mangostin was caused by exacerbates TNF- α secretion by LPS-treated cultures of human monocyte-derived macrophages (MDM) and attenuates secretion of inflammatory mediators in activated human

1.3 Literature review anti-acne activity of α -mangostin

In 1983, Sundaram *et al.* [6] studied antimicrobial activities of *Garcinia mangostana* by cup plate and streak plate methods. The result showed that mangostin could inhibit 7 types of bacteria including *Staphylococcus aureus*, *Pseudomonas aeruginosa*, *Salmonella typhimurium*, *Bacillus subtilis*, *Proteus mirabilis*, *Klebsiella pneumoniae* and *Escherichia coli* with the MIC varied from 12.5 μ g/mL to 50 μ g/mL.

In 2005, Chomnawang *et al.* [4] studied effects of mangostin against acne-inducing bacteria. The results show that mangostin can inhibit *Propionibacterium acnes* and *Staphylococcus epidermidis* with the same minimum inhibitory concentration (MIC) values of 0.039 mg/mL.

In 2009, Pothitirat *et al.* [22] studied anti-acne activities of bioactive constituents in young and mature *Garcinia mangostana* fruit rind. They found that the mature fruit rind extract promoted anti-acne inducing bacteria better than the extract from the young fruit rinds. The mature fruit rind extract had a higher content of α -mangostin than the young fruit rind extract.

1.4 Objective and scope of work

Objective:

To solve the problem of low water solubility by creating a novel water-dispersible α -mangostin particles.

Scope of work:

1. Preparation of water-dispersible α -mangostin particles.
2. Characterization of the obtained water-dispersible α -mangostin particles.
3. Biological activity testing of the obtained water-dispersible α -mangostin particles.



CHAPTER II

EXPERIMENTAL

2.1 Materials and Chemicals

α -Mangostin (94% of α -mangostin) was purchased from Welltech biotechnology (Bangkok, Thailand). Polyethylene glycol (MW 35000 g/mol, PEG35000), hydrogen peroxide (H_2O_2) and potassium dihydrogen phosphate (KH_2PO_4) were purchased from Merck (Darmstadt, Germany). Horseradish peroxidase (HRP) was purchased from Chemieliva pharmaceutical company (Chongqing, China). Polyethylene glycol (MW 200 g/mol, PEG200), polyethylene glycol (MW 400 g/mol, PEG400), polyethylene glycol (MW 600 g/mol, PEG600), polyethylene glycol (MW 950 g/mol, PEG950) and polyethylene glycol (MW 2050 g/mol, PEG2050), bromobutane were purchased from Acros organics (Geel, Belgium). Potassium carbonate (K_2CO_3) was purchased from Sigma-Aldrich (Streinheim, Germany). Methanol, ethanol, propanol, butanol, acetone and dimethyl sulfoxide were purchased from RCI labscan (Bangkok, Thailand). Disodium hydrogen phosphate (Na_2HPO_4) was purchased from Carlo erba reagent (Cornaredo, Italy).

2.1.1 Media culture and chemical reagent for cell culture and treatment

RAW 264.7 cell line was purchased from the global bioresource center (ATCC, Manassas, Virginia, USA). Dulbecco's modified eagle medium (DMEM), fetal bovine serum (FBS), sodium pyruvate and 4-(2-hydroxyethyl)-1-piperazineethanesulfonic acid (HEPES) were purchased from Hyclone (Utah, USA). Sodium nitrite ($NaNO_2$) and sulfanilamide were purchased from Merck (Darmstadt, Germany). Budesonide, N-1-

naphthylethylenediamine dihydrochloride (NED) and ipopolysaccharide (LPS) were purchased from Sigma-Aldrich (Steinheim, Germany). 3-(4 5-dimethylthiazol-2-yl)-2 5-diphenyltetrazolium bromide (MTT) was purchased from USB Corporation (Ohio, USA).

2.1.2 Media culture for anti-acne study

Propionibacterium acnes (*P. acnes*, ATCC 6919) was obtained from the Department of Medical Sciences, Ministry of Public Health (Thailand). Brain heart infusion broth (BHI broth) and brain heart infusion agar (BHI agar) were purchased from HiMedia Laboratory (Mumbai, India). AnaeroPack was purchased from Mitsubishi Gas Chemical Company (Tokyo, Japan).

2.2 Instruments and Equipment

Freeze-drying was carried out on a vacuum freeze dryer (Labconco corporation, Kansas, MI, USA). The morphology of dry products was examined by scanning electron microscopy (SEM; JSM-IT100 JEOL, Tokyo, Japan). Particle size and size distributions from SEM were measured using Image J software. UV-Visible absorption was carried out by UV-visible spectrometer (Optizen POP QX, Korea). The IR spectrum was acquired using FT-IR spectrophotometer (Nicolet 6700, Thermo Electron Corporation, Madison, WI, USA) in ATR (Attenuated Total Reflectance) mode. Size distribution and zeta potential were examined by dynamic light scattering (DLS) using zetasizer nano series instrument (Zs, Malvern Instruments, United Kingdom). Thermogravimetric analysis was performed with thermogravimetric analyzers (Netzsch STA 449 F1, Germany). Crystallinity of particles was determined by powder X-ray diffraction (XRD) on a Rigaku X-ray diffractometer DMAX 2200/Ultima (Japan). The functional groups on the surface of

particles were analyzed by X-ray photoelectron spectroscopy (XPS) using Kratos X-ray photoelectron spectrometer (Axis-Ultra DLD XSAM800, Europe).

2.3 Optimization process for preparing of water dispersible α -mangostin

2.3.1 Preparation of phosphate buffer

Potassium dihydrogen phosphate (KH_2PO_4 , 0.24 g) and disodium hydrogen phosphate (Na_2HPO_4 , 1.44 g) were dissolved in 1000 mL of DI water. After that, the solution was adjusted pH value to 7.4 using 0.1 M hydrochloric acid.

2.3.2 Preparation of water dispersible α -mangostin through enzymatic template polymerization

Water dispersible α -mangostin was prepared through polymerization reaction using Pukfukdee's protocol [18]. α -Mangostin (84.3 mg) was dissolved in 16.9 mL of ethanol, under vigorous stirring. Then, polyethylene glycol (PEG, 7.5 mg) was added. After that, horseradish peroxidase (HRP, 0.25 mg), hydrogen peroxide (30% H_2O_2 , 2.0 mL) and phosphate buffer (10 mM of PO_4^{3-} , pH 7.4, 16.9 mL) were added to the mixture. The reaction was stirred at the ambient temperature for 48 h. The reaction was worked up and purified by dialysis against water with dialysis tubing cellulose membrane (molecular weight cut-off = 14,000) to give a yellow suspension. The suspension was freeze-dried. Finally, the product (pMG) was obtained as a yellow product.

2.3.2.1 Effect of enzyme

To study the effect of enzyme on particles formation, various amounts of HRP were studied (Table 2.1).

Table 2.1 The experimental conditions for study effect of enzyme.

Entry	Amount of α -MG (mg)	Amount of PEG (MW = 35000) (mg)	Amount of HRP (mg)	Amount of H ₂ O ₂ (mL)	Amount of ethanol (mL)	Amount of phosphate buffer (mL)
1	84.3	7.5	-	2.0	16.9	16.9
2	84.3	7.5	0.25	2.0	16.9	16.9
3	84.3	7.5	0.50	2.0	16.9	16.9
4	84.3	7.5	1.00	2.0	16.9	16.9
5	84.3	7.5	2.50	2.0	16.9	16.9
6	84.3	7.5	3.75	2.0	16.9	16.9

2.3.2.2 Effect of polymer

To study the effect of molecular weight of polyethylene glycol (PEG) on particles formation, various molecular weights of PEG were studied (Table 2.2).

Table 2.2 The experimental conditions for study effect of polymer.

Entry	Amount of α -MG (mg)	PEG		Amount of HRP (mg)	Amount of H ₂ O ₂ (mL)	Amount of ethanol (mL)	Amount of phosphate buffer (mL)
		Molecular weight of PEG (g/mol)	Amount of PEG (mg)				
1	84.3	-		0.25	2.0	16.9	16.9
2	84.3	200	7.5	0.25	2.0	16.9	16.9
3	84.3	400	7.5	0.25	2.0	16.9	16.9
4	84.3	600	7.5	0.25	2.0	16.9	16.9
5	84.3	950	7.5	0.25	2.0	16.9	16.9
6	84.3	2,050	7.5	0.25	2.0	16.9	16.9
7	84.3	35,000	7.5	0.25	2.0	16.9	16.9

2.3.2.3 Effect of oxidizing agent

To study the effect of oxidizing agent on particles formation, various amounts of oxidizing agent were studied (Table 2.3).

Table 2.3 The experimental conditions for study effect of oxidizing agent.

Entry	Amount of α -MG (mg)	Amount of PEG (mg)	Amount of HRP (mg)	Amount of H ₂ O ₂ (mL)	Amount of ethanol (mL)	Amount of phosphate buffer (mL)	The obtained [H ₂ O ₂] %(v/v)
1	84.3	7.5	0.25	-	16.9	16.9	0
2	84.3	7.5	0.25	2.0	16.9	16.9	6
3	84.3	7.5	0.25	2.6	16.9	16.9	8
4	84.3	7.5	0.25	3.3	16.9	16.9	10
5	84.3	7.5	0.25	5.0	16.9	16.9	15

2.4 Self-assembly of α -mangostin

2.4.1 Preparation of water dispersible α -mangostin particles through self-assembly process

Water-dispersible α -mangostin particles were prepared using just ethanol and DI water as follow: α -mangostin (75.0 mg) was dissolved in ethanol (7.5 mL). Then DI water (7.5 mL) was dropped into the solution. The nanoparticles were formed and ethanol was removed under vacuum at 30°C with evaporation rate of 0.15-0.3 mL/min to give a yellow suspension. The suspension was dried using vacuum freeze dryer for a period of 48 h. α -Mangostin particles was obtained as a yellow solid. ¹H NMR (400 MHz, DMSO-d₆, Figure

3.8, δ ppm) 1.59 (s, 6H, 19- and 20-CH₃), 1.70 (s, 3H, 15-CH₃), 1.75 (s, 3H, 14-CH₃), 3.18 (d, $J = 7.0$ Hz, 2H, 16-H), 3.67 (s, 3H, 7-OMe), 3.99 (d, $J = 6.2$ Hz, 2H, 11-H), 5.15 (s, 2H, 12- and 17-H), 6.31 (s, 1H, 4-H), 6.77 (s, 1H, 5-H) and 13.70 (s, 1H, C-1-OH). ATR FT-IR (cm⁻¹): 3385.9 (brd, O-H stretching), 2962.5, 2914.5, 2858.3 (m, C-H stretching of saturated carbons), 1643.4 (str, C=O stretching of aromatic ketone), 1605.1, 1580.4 (str, C=C stretching of aromatic ring), 1461.4, 1432.6 (str, C-H bending of methyl groups), 1373.4 (str, C-H bending of gem dimethyl), 1278.2 (str, C-O-C stretching of methoxy group on benzene ring), 1226.8 (str, C-O stretching of vinyl ether), 1184.1, 1154.2 and 1078.7, 1044.1 (str, C-O stretching of C-O connected on hydroxyl groups). UV-Visible absorption (λ_{\max} nm in ethanol): 248 ($\pi - \pi^*$ transition) and 321 (n - π^* transition).

2.4.1.1 Effect of α -mangostin concentration used

To study the effect of concentration of α -mangostin used on α -mangostin particles formation, various concentrations of α -mangostin were studied (Table 2.4).

Table 2.4 Amounts of materials used in the preparation of α -mangostin particles.

Entry	α -Mangostin (mg)	Ethanol (mL)	Starting [α -mangostin] in ethanol (%w/v)	Water (mL)	Final [α -mangostin] in the obtained suspension (%w/v)	Amount of ethanol (%v/v) in water
1	25.0	1.0	2.5	4.0	0.5	20.0
2	50.0	1.0	5.0	4.0	1.0	20.0
3	250.0	1.0	25.0	4.0	5.0	20.0
4	500.0	1.0	50.0	4.0	10.0	20.0
5	1500.0	1.0	150.0	4.0	30.0	20.0

2.4.1.2 Effect of ethanol ratio

To study the effect of ratio of ethanol on α -mangostin particles formation, various amounts of ethanol were studied (Table 2.5).

Table 2.5 Amounts of materials used in the preparation of α -mangostin particles.

Entry	α -Mangostin (mg)	Ethanol (mL)	Starting [α -mangostin] in ethanol (%w/v)	Water (mL)	Final [α -mangostin] in the obtained suspension (%w/v)	Amount of ethanol (%v/v) in water
1	25.0	0.025	100.0	4.80	0.5	0.5
2	25.0	0.25	10.0	4.75	0.5	5.0
3	25.0	1.0	2.5	4.0	0.5	20.0
4	25.0	2.5	1.0	2.5	0.5	50.0

2.4.1.3 Effect of the type of organic solvent used for dissolving α -mangostin

To study the effect of the type of organic solvent on particle formation, various organic solvents including dimethyl sulfoxide (DMSO), methanol, propanol, butanol and acetone were studied. The results of all products were examined by SEM.

α -Mangostin particles obtained from process using 50% v/v of propanol in water (nMG-P): ^1H NMR (400 MHz, DMSO- d_6 Figure 3.8, δ ppm) 1.59 (s, 6H, 19- and 20- CH_3), 1.70 (s, 3H, 15- CH_3), 1.74 (s, 3H, 14- CH_3), 3.17 (d, $J = 6.4$ Hz, 2H, 16-H), 3.67 (s, 3H, 7-OMe), 3.98 (d, $J = 6.2$ Hz, 2H, 11-H), 5.14 (s, 2H, 12- and 17-H), 6.30 (s, 1H, 4-H), 6.76 (s, 1H, 5-H) and 13.69 (s, 1H, C-1-OH). ATR FT-IR (cm^{-1}): 3393.5 (brd, O-H stretching), 2963.1, 2913.0, 2856.9 (m, C-H stretching of saturated carbons), 1642.6 (str, C=O stretching of aromatic ketone), 1605.3, 1579.9 (str, C=C stretching of aromatic ring), 1460.7, 1432.5 (str, C-H bending of methyl groups), 1373.5 (str, C-H bending of gem

dimethyl), 1278.1 (str, C-O-C stretching of methyl groups on benzene ring), 1225.6 (str, C-O stretching of vinyl ether), 1184.0, 1154.3 and 1077.9, 1044.0 (str, C-O stretching of C-O connected on hydroxyl groups). UV-Visible absorption (λ_{\max} nm in ethanol): 248 (π - π^* transition) and 321 (n - π^* transition).

α -Mangostin particles obtained from process using 50% v/v of butanol in water (nMG-B): ^1H NMR (400 MHz, DMSO- d_6 , Figure 3.8, δ ppm) 1.59 (s, 6H, 19- and 20- CH_3), 1.70 (s, 3H, 15- CH_3), 1.74 (s, 3H, 14- CH_3), 3.17 (d, $J = 6.7$ Hz, 2H, 16-H), 3.67 (s, 3H, 7-OMe), 3.97 (d, $J = 6.7$ Hz, 2H, 11-H), 5.14 (s, 2H, 12- and 17-H), 6.30 (s, 1H, 4-H), 6.76 (s, 1H, 5-H) and 13.69 (s, 1H, C-1-OH). ATR FT-IR (cm^{-1}): 3394.3 (brd, O-H stretching), 2963.0, 2923.4, 2857.8 (m, C-H stretching of saturated carbons), 1642.2 (str, C=O stretching of aromatic ketone), 1605.3, 1579.8 (str, C=C stretching of aromatic ring), 1460.3, 1432.4 (str, C-H bending of methyl groups), 1373.6 (str, C-H bending of gem dimethyl), 1278.1 (str, C-O-C stretching of methyl groups on benzene ring), 1225.9 (str, C-O stretching of vinyl ether), 1184.1, 1154.2 and 1078.1, 1043.9 (str, C-O stretching of C-O connected on hydroxyl groups). UV-Visible absorption (λ_{\max} nm in ethanol): 248 (π - π^* transition) and 321 (n - π^* transition).

2.5 Self-assembly of α -mangostin derivative

2.5.1 Synthesis of α -mangostin derivative

α -Mangostin (100.0 mg, 0.244 mmol) was dissolved in 10 mL of acetone, under stirring. Then, potassium carbonate (168.6 mg, 1.22 mmol) and bromobutane (79.0 μL , 0.732 mmol) were added to the solution. The mixture was refluxed at 80°C for 72 h. The

solution was cooled at room temperature. After that, dichloromethane (20 mL) was added to the mixture. The reaction mixture was extracted with water (3x20 mL) to remove the remained potassium carbonate. The organic layer was dried over sodium sulfate. After filtration, organic layer was removed under vacuum. The brownish derivative α -mangostin (dMG) was obtained with 79% yield. ^1H NMR (400 MHz, CDCl_3 , Figure 3.17, δ ppm) 0.89 (t, $J = 6.6$ Hz, 6H, d'-H), 1.56 – 1.45 (m, 4H, c'-H), 1.68 (s, 6H, 19- and 20- CH_3), 1.80 (s, 3H, 15- CH_3), 1.85 (s, 3H, 14- CH_3), 2.17 (s, 4H, b'-H), 3.36 (d, $J = 7.0$ Hz, 2H, 16-H), 3.80 (s, 3H, 7-OMe), 4.05 (m, 4H, a'-H), 4.13 (d, $J = 6.4$ Hz, 2H, 11-H), 5.25 (s, 2H, 12- and 17-H), 6.29 (s, 1H, 4-H), 6.71 (s, 1H, 5H) and 13.51 ppm (s, 1H, C-1-OH).

2.5.2 Preparation of α -mangostin derivative (dMG) through self-assembly process

α -Mangostin derivative (dMG, 75.0 mg) was dissolved in ethanol (7.5 mL). Then DI water (7.5 mL) was dropped into the solution. Ethanol was then removed from the suspension under vacuum at 30°C with evaporation rate of 0.15-0.3 mL/min. The suspension was freeze dried for a period of 48 h. The product was obtained as a brown solid. Then, morphology of the obtained dry product was examined by scanning electron microscopy (SEM)

2.6 Anti-inflammatory activity and cell viability

In vitro anti-inflammatory property of the original α -mangostin and nMG-E were tested with RAW 264.7 cells. Nitric oxide assay [23] was used to evaluate anti-inflammatory activity and MTT assay [24] was used to evaluate cell viability.

2.6.1 Preparation of complete media

Complete media 40 mL was prepared by mixing fetal bovine serum (FBS, 4.0 mL), antibiotic (gentamicin, 400 μ L), 4-(2-hydroxyethyl)-1-piperazineethanesulfonic acid (HEPES, 400 μ L), sodium pyruvate (400 μ L) and dulbecco's modified eagle medium DMEM (34.8 mL).

2.6.2 Preparation of tested sample

The stock suspensions of the original α -mangostin and nMG-E (4,000 ppm) were prepared by dissolved sample (10.0 mg) in milli-Q water (2.50 mL). The stock suspensions were sterilized by autoclaving at 121°C for 15 minutes. Then, the stock suspension was diluted with cell culture to 30.00, 22.50, 16.88, 12.66, 9.50 and 1.25 mg/mL, respectively.

2.6.3 Preparation of Nitrite standards for standard curve

The stock solution of NO²⁻ standard (100,000 ppm) was prepared by dissolved sodium nitrite (100.0 mg) in milli-Q water (1.00 mL). Then, the stock solution of NO²⁻ standard was diluted with complete media to 100.0, 50.0, 25.0, 12.5, 6.25, 3.125 and 1.56 ppm, respectively by using two-flow dilution.

2.6.4 Cell culture conditions and cell treatment

RAW 264.7 cells were cultured in a humidified atmosphere of 5% CO₂ with complete media (2.6.1) at 37°C for 72 h. Then RAW264.7 cells were seeded at 1×10^4 cell/well in 96 well plates for overnight. After that supernatant was removed and replaced with tested sample 50 μ l/well and pretreat for 1 h. After pretreatment, complete media contained LPS (200 ng/mL) and IFN- γ (20 ng/mL) were added 50 μ l/well (the final concentrations of LPS and IFN- γ are 100 and 10 ng/ml, respectively) and incubated for

24 h. Then, the supernatant was subjected to nitric oxide assay (2.6.5). The remaining cells on the plate were subjected to MTT assay (2.6.6).

2.6.5 Determination of nitric oxide production using nitric oxide assay

The supernatant of cell treatment from 2.6.4 was subjected to nitrite production by transferring to u-bottom 96 well plate (50 μ L/well). Then 1%w/v sulfanilamide in 5%v/v phosphoric acid in water was added into the supernatant 50 μ L/well and incubated in the dark at room temperature for 5 min. After that, 0.1%w/v NED solution in water was added 50 μ L/well and incubated in the dark at room temperature for 5 min. The mixture was subjected to UV absorption spectroscopy by microplate reader at 540 nm using complete media as a blank. The absorbance was used to quantify nitrite concentration from a sodium nitrite standard curve (Figure A2, Appendix). The obtained nitrite concentration of the tested samples was calculated as the percentage of nitric oxide production compared with the nitrite concentration of water, as follows:

$$\%NO \text{ production} = \frac{\text{Nitrite concentration of the tested sample}}{\text{Nitrite concentration of water}} \times 100$$

2.6.6 Determination of cell viability using MTT assay

The supernatant of remaining cells on the plate from 2.6.4 was removed and replaced with complete media (100 μ L/well). Then cells were treated with 0.5%w/v MTT solution (in phosphate buffer saline) 10 μ L/well and incubated in a humidified atmosphere at 37°C for 4 h. After 4 h, the purple formazan sediment was obtained from the reduction of MTT by mitochondrial dehydrogenase of living cells [24]. The obtained purple formazan sediment was dissolved completely using DMSO (200 μ L/well) and incubated in the dark

at room temperature for 5 min. The absorbance of MTT metabolic product was measured at 540 nm by microplate reader using complete media as a blank. The obtained absorbance was calculated as the percentage of cell viability, as follows:

$$\% \text{Cell viability} = \frac{\text{OD sample} - \text{OD media}}{\text{OD water} - \text{OD media}} \times 100$$

Where OD sample is the absorbance of cells treated with sample and MTT reagent; OD water is the absorbance of cells treated with water and MTT reagent; and OD media is the absorbance of untreated cells, but treated with MTT reagent.

2.7 Anti-acne activity

Anti-acne activity of the nMG-E was determined by measuring clear inhibition zone using agar disc diffusion method [25].

2.7.1 Preparation of brain heart infusion broth

The brain heart infusion broth (BHI broth, 3.8%w/v) was prepared by adding BHI broth (18.5 g) and DI water (481.5 mL) into duran glass bottle. Then the mixture was sterilized by autoclaving at 121°C for 15 minutes.

2.7.2 Preparation of brain heart infusion agar base

The brain heart infusion agar (BHI agar, 5.5%w/v) was prepared by adding BHI agar 26.0 g and DI water (474.0 mL) into erlenmeyer flask. The mixture was sterilized by autoclaving at 121°C for 15 minutes. The obtained molten BHI agar was cooled to 50°C before poured on the sterile petri plate (20 mL/plate), and allow the agar to setly leaving at room temperature.

2.7.3 Preparation of tested sample

A stock solution of the original α -mangostin (20.0 mg/mL) were prepared by dissolving 20.0 mg of α -mangostin in 50.00 μ L of DMSO and 950 μ L of milli-Q water, then stock solution of the original α -mangostin was diluted in 5% v/v DMSO in milli-Q water to 10.0, 5.0, 2.5 and 1.25 mg/mL, respectively by using two-folds dilution. The stock suspensions of nMG-E, nMG-P and nMG-B were prepared by dispersing 20.0 mg of each material in 1.00 mL of pure milli-Q water, then the stock suspensions were diluted in milli-Q water to 10.0, 5.0, 2.5 and 1.25 mg/mL, respectively by using two-folds dilution.

2.7.4 Bacterial culture and treatment

Propionibacterium acnes (*P. acnes*, 20 μ L) were incubated in BHI broth (980 μ L) under anaerobic condition for 72 h at 37°C before being adjusted to approximately cell density of 1×10^8 CFU/mL (0.5 McFarland standard). Then the obtained *P. acne* (75 μ L) was coated on the agar base plate (2.7.2) and a sterile paper disc (6 mm) was placed on the surface of agar. The tested sample (20 μ L) was dropped on the disc and plates were incubated at 37°C for 72 h under anaerobic condition. Finally, the clear inhibition zone was measured in millimeter (mm).

CHAPTER III

RESULTS AND DISCUSSIONS

3.1 Optimizing the preparation of water dispersible α -mangostin

First, water dispersible α -mangostin particles were prepared using Pukfukdee protocol [18] via enzymatic template polymerization reaction with PEG as polymer, horseradish peroxidase (HRP) as enzyme and hydrogen peroxide (H_2O_2) as oxidizing agent. To optimize the reaction conditions, the effect of enzyme, polymer and amount of oxidizing agent were studied. The obtained dry product made of enzymatic template polymerization was subjected to morphology and particle size analysis.

We observed the effect of the enzyme on particles formation. The SEM images (Figure 3.1) show that amount of HRP enzyme at 0.003x, 0.006x, 0.012x, 0.030x and 0.045x of α -mangostin lead to spherical particle products with the particle size of 1286.12 ± 370.29 , 1539.56 ± 773.19 , 1453.07 ± 505.96 , 1446.05 ± 460.56 and 1157.51 ± 347.92 nm, respectively. In addition, we noticed that in the absence of an enzyme, the spherical particle product still formed. These results indicate that the enzyme is not essential for α -mangostin particles formation.

Next, we evaluated the effect of the polymer on particles formation. The SEM images (Figure 3.2) show that the particle size of products obtained when using molecular weight of PEG of 200, 400, 600, 950, 2050 and 35000 g/mol are 1718.20 ± 672.71 , 1354.54 ± 822.83 , 1317.62 ± 581.19 , 1329.12 ± 532.37 and 1286.12 ± 370.29 nm, respectively. Also, we found that in the absence of polymer in the reaction, the spherical particle

product still formed. These results indicate that the polymer is not essential for α -mangostin particles formation.

Then, we studied the effect of oxidizing agent on particles formation. The SEM images (Figure 3.3) show that the particle size of products obtained when using the amount of H_2O_2 of 6, 8, 10 and 15 % v/v are 1286.12 ± 370.29 , 1002.91 ± 240.64 , 1012.86 ± 416.93 and 1296.02 ± 262.58 nm, respectively. Besides, we found that in the absence of oxidizing agent in the reaction, the spherical particle product still formed. These results indicate that the oxidizing agent is not essential for α -mangostin particles formation.

Interestingly, enzyme, polymer and oxidizing agent are not essential for α -mangostin particles formation. It was likely that the α -mangostin particles were not formed by the enzymatic template polymerization reaction. To confirm this presumption, the dry pMG product obtained from using the molecular weight of PEG at 35,000 g/mol, HRP enzyme at 0.25 mg and H_2O_2 at 6% v/v was dissolved in DMSO-d_6 and subjected to analyze by NMR spectroscopy.

The chemical shift of the pMG product (Figure 3.4) is the same to those of the original α -mangostin solid. This result supports that the α -mangostin particles were not the product of the enzymatic template polymerization, but a self-assembly product.

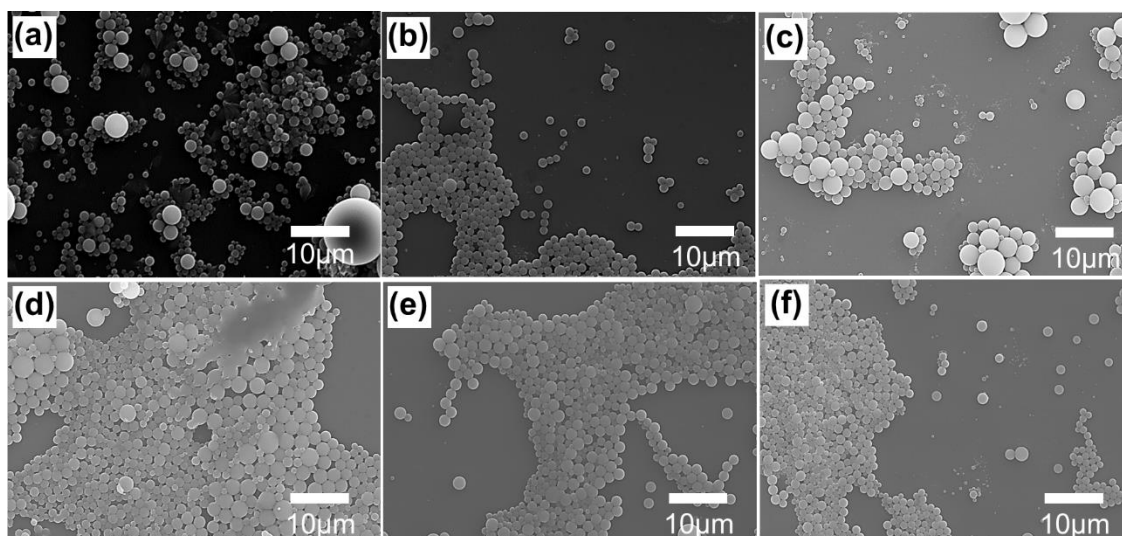
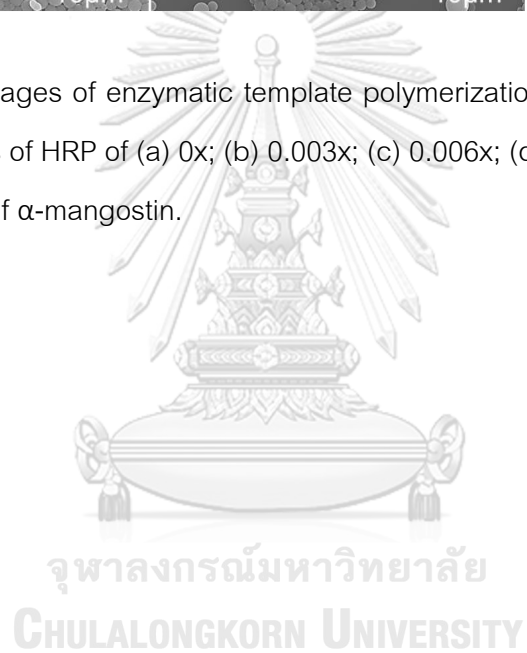


Figure 3.1 SEM images of enzymatic template polymerization products obtained at the amounts of HRP of (a) 0x; (b) 0.003x; (c) 0.006x; (d) 0.012x; (e) 0.030x and (f) 0.045x of α -mangostin.



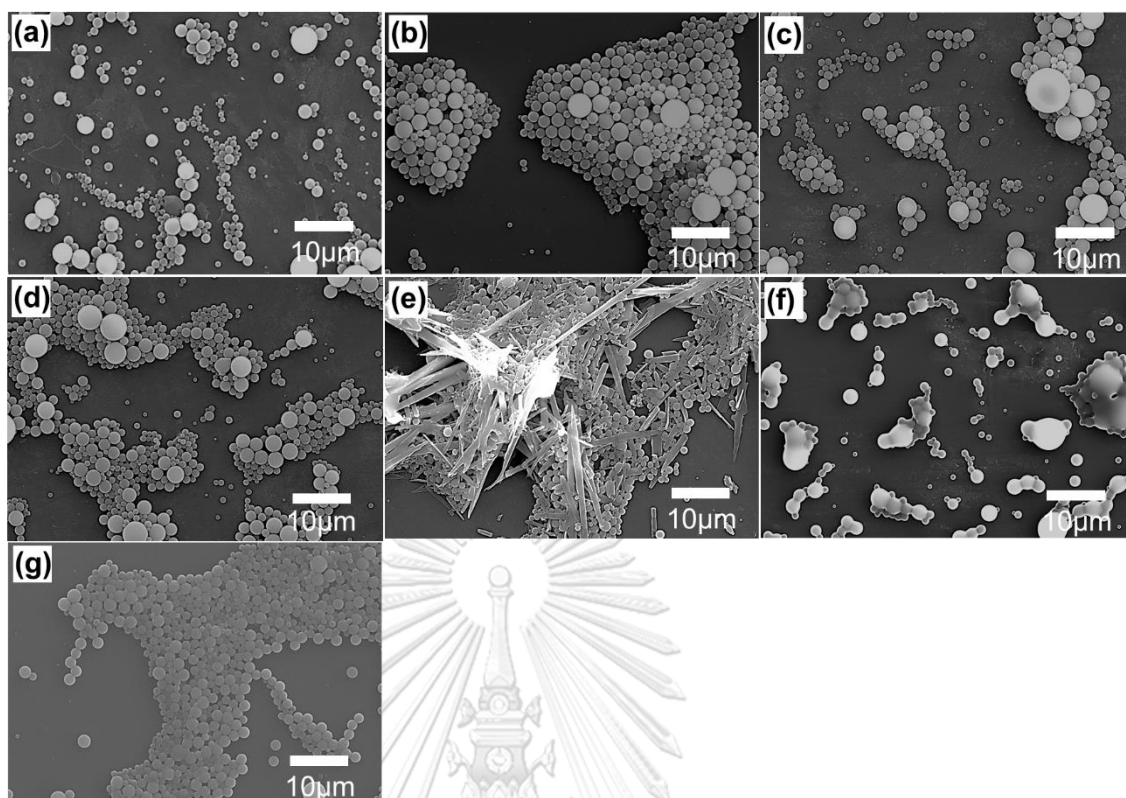


Figure 3.2 SEM images of enzymatic template polymerization products obtained at the molecular weights of PEG of (a) 0; (b) 200; (c) 400; (d) 600; (e) 950; (f) 2050 and (g) 35000 g/mol.

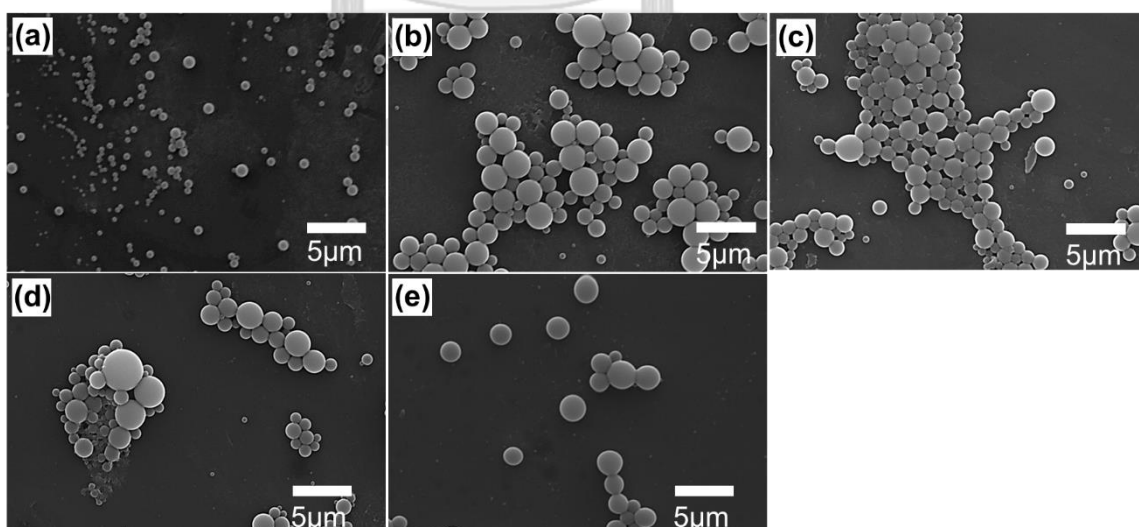


Figure 3.3 SEM images of enzymatic template polymerization products obtained at the amounts of H_2O_2 of (a) 0; (b) 6; (c) 8; (d) 10 and (e) 15 % v/v.

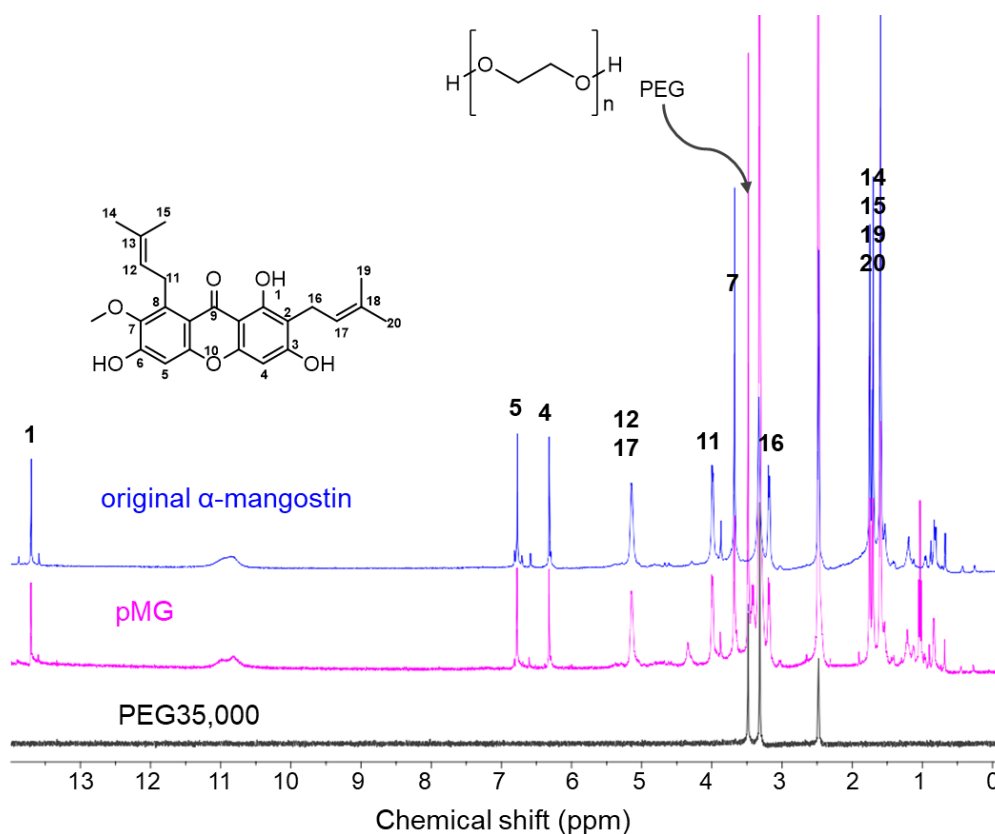


Figure 3.4 NMR spectra of the original α -mangostin solid, enzymatic template polymerization products (pMG) obtained at the molecular weight of PEG at 35,000 g/mol, HRP enzyme at 0.25 mg and H_2O_2 at 6% v/v, and PEG35,000 in CDCl_3 .

จุฬาลงกรณ์มหาวิทยาลัย
CHULALONGKORN UNIVERSITY

3.2 Self-assembly of α -mangostin

The water-dispersible α -mangostin particles were prepared by a new discovery process using just ethanol and deionized water (DI water). To optimize the self-assembly conditions, the effect of α -mangostin concentration used, ethanol/water ratio and type of organic solvent used for dissolving α -mangostin, on particle formation were studied. The obtained dry product was subjected to morphology and particle size analysis by SEM.

The condition that gave the most uniform particle and gave particle size in the range of 200-600 nm (for skin application, [15-17]) was selected as the best condition.

First, we studied the effect of α -mangostin concentration used on particles formation. The SEM images (Figure 3.5) show that the spherical structure of water dispersible particles was obtained when using the α -mangostin concentration at 0.5, 1.0 and 5.0% w/v, only. The result reveals that the particle size increased with increasing α -mangostin concentration. But, when the α -mangostin concentration reached 10% w/v and above 10% w/v, α -mangostin particles could not form. The increase in particle size at higher α -mangostin concentration could be understood base on the increased amount of α -mangostin molecules in a fixed ethanol volume. We assumed that when the amount of α -mangostin molecules increased, the distance between each molecule was shorter, leading to more accumulation of the molecules which resulting in giant particles. Therefore, to get an appropriate particle size for skin application, we selected the concentration of α -mangostin at 0.5% w/v for further study.

Next, we evaluated the effect of ethanol/water ratio on particles formation by preparing α -mangostin particles from various ethanol/water ratios. The SEM images (Figure 3.6) show that the particle sizes of products obtained when using the amount of ethanol at 0.5, 5.0, 20.0 and 50.0% v/v are 865.70 ± 134.35 , 686.49 ± 133.24 , 595.99 ± 366.38 and 312.17 ± 55.11 nm, respectively. We found that the particle size of the particles decreased as the ethanol content increased. The decrease in particle size at higher ethanol content could be explained similar to the effect of α -mangostin concentration. In

this study, the particles obtained at 50% ethanol in water (nMG-E) gave the most uniform particle. Thus this condition was selected.

In addition, we investigated the effect of the type of organic solvent used for dissolving α -mangostin at the beginning of the process. Here ethanol was replaced with dimethyl sulfoxide, methanol, propanol, butanol and acetone. The SEM images (Figure 3.7) show that only propanol and butanol gave spherical particles of α -mangostin. The particle size of particles obtained from using propanol and butanol are 324.35 ± 71.45 and 467.97 ± 188.51 nm, respectively.

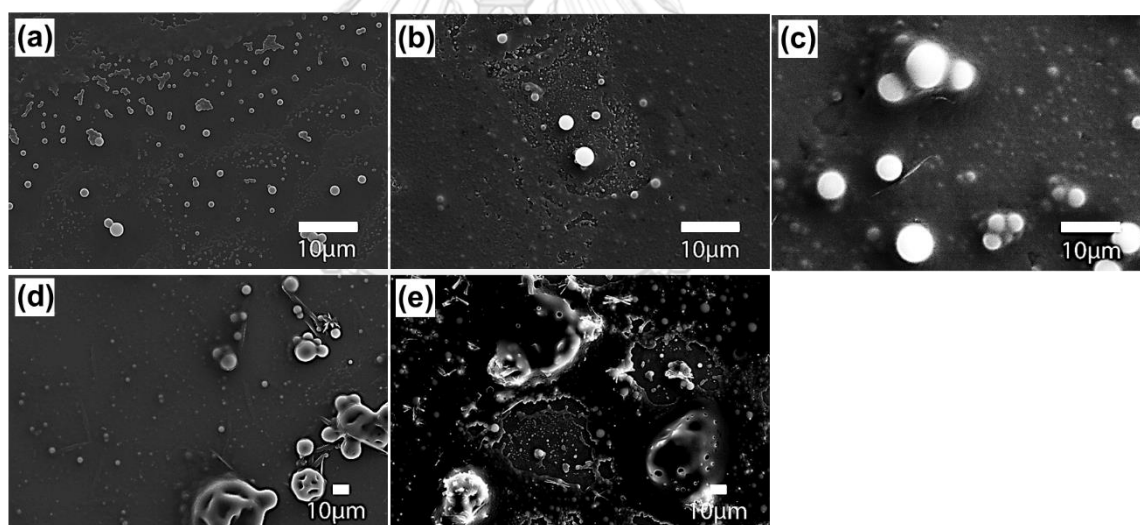


Figure 3.5 SEM images of α -mangostin nanoparticles obtained when using α -mangostin concentration at (a) 0.5; (b) 1.0; (c) 5.0; (d) 10.0 and (e) 30.0% w/v.

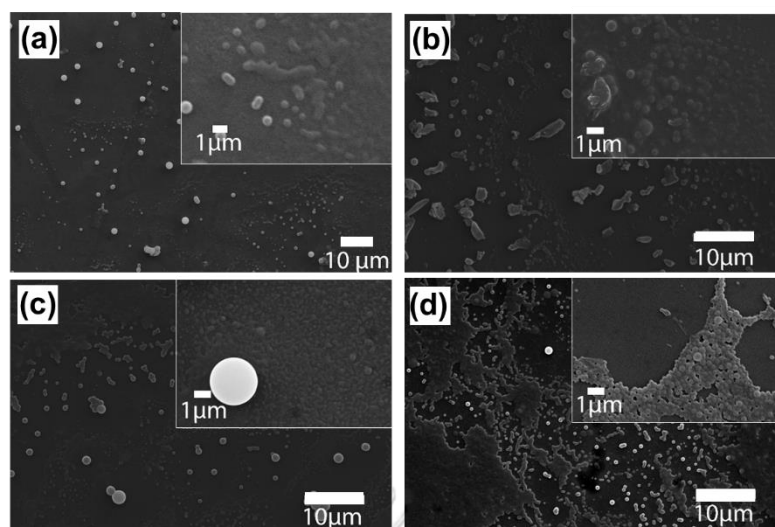


Figure 3.6 SEM images of α -mangostin nanoparticles obtained when using amount of ethanol at (a) 0.5; (b) 5.0; (c) 20.0 and (d) 50.0% v/v.

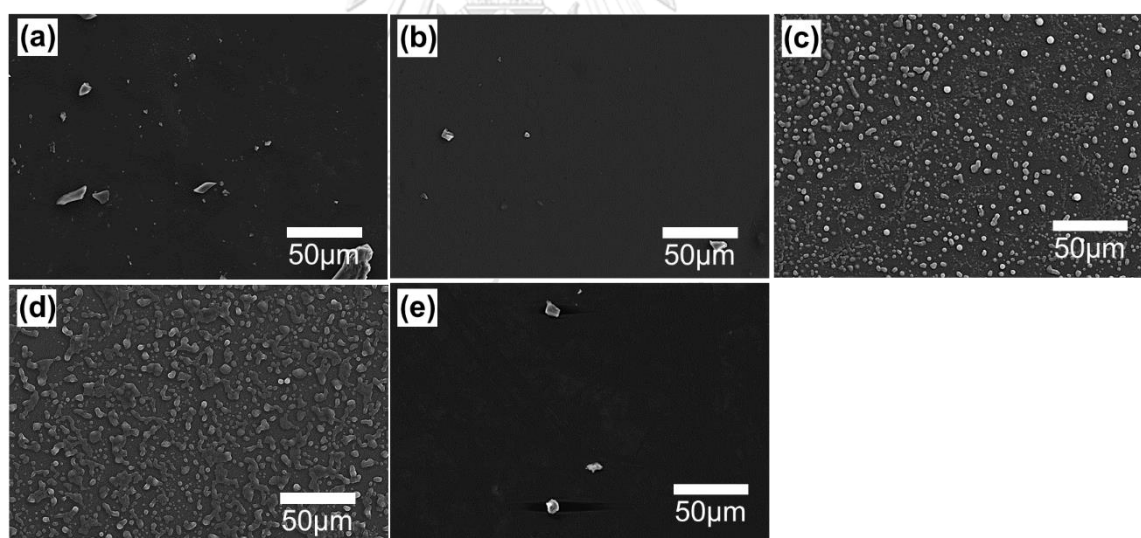


Figure 3.7 SEM images of α -mangostin nanoparticles obtained when using (a) dimethyl sulfoxide; (b) methanol; (c) propanol; (d) butanol and (e) acetone as the organic solvent for dissolving α -mangostin replace ethanol.

3.2.1 Chemical structure of α -mangostin nanoparticles

The nMG-E, nMG-P nMG-B particles and original α -mangostin solid were subjected to chemical structure analysis by ^1H NMR spectroscopy. ^1H NMR spectra of all three particles (dissolving as the solution in DMSO-d_6 , Figure 3.8) are similar to that of the original α -mangostin solid. Indicating that no chemical transformation was taking place to the α -mangostin molecule structure during the particle formation process.

In addition, we compared the solid-state ^1H NMR between nMG-E and the original α -mangostin solid. The solid-state ^1H NMR spectra of nMG-E (Figure 3.9) shown the same pattern to the original α -mangostin solid, but the chemical shift of nMG-E slightly shift from the original α -mangostin. Because the dipole-dipole coupling between nuclei is prominent in solid state NMR, and such coupling is directly influenced by molecular arrangement of the material, it is likely that the small difference in chemical shift of nMG-E and of the original α -mangostin reflects the different molecular arrangement between the two materials.

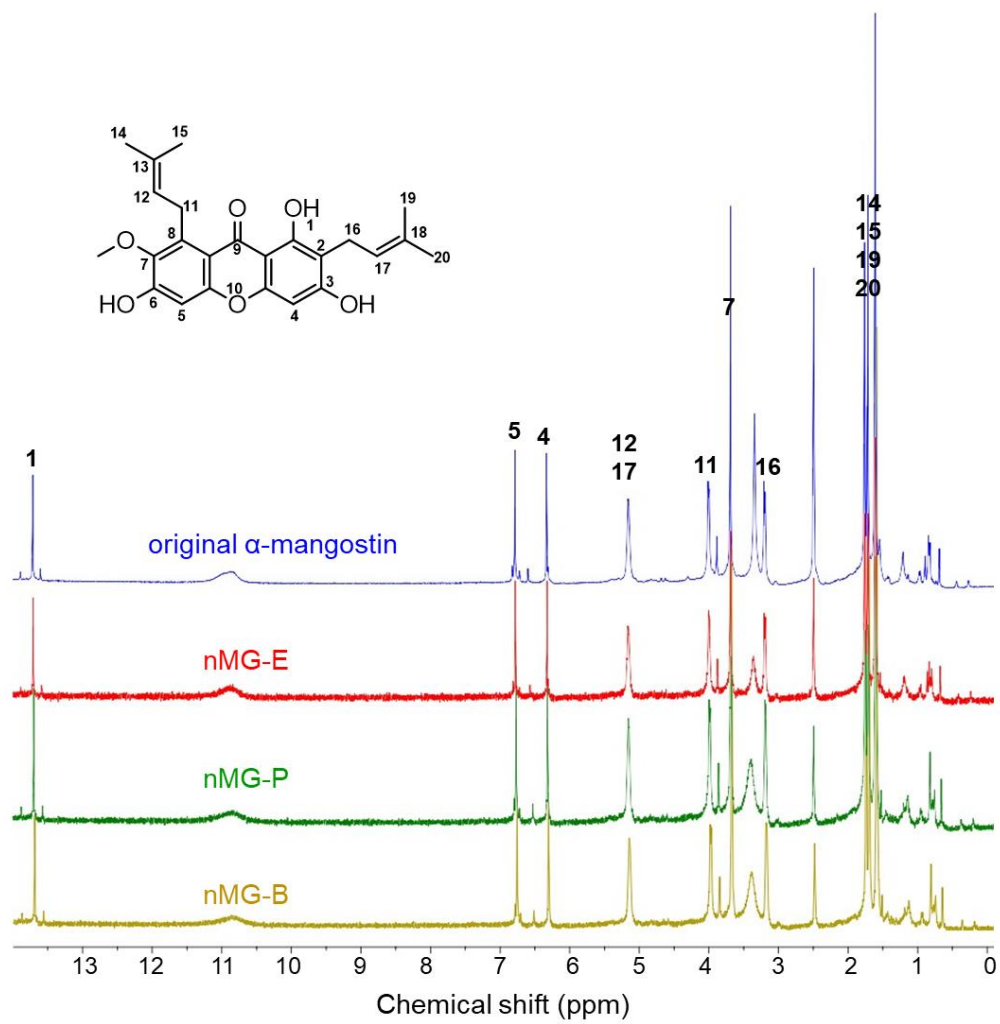


Figure 3.8 NMR spectra of the original α -mangostin solid, nMG-E, nMG-P and nMG-B in DMSO- d_6 .

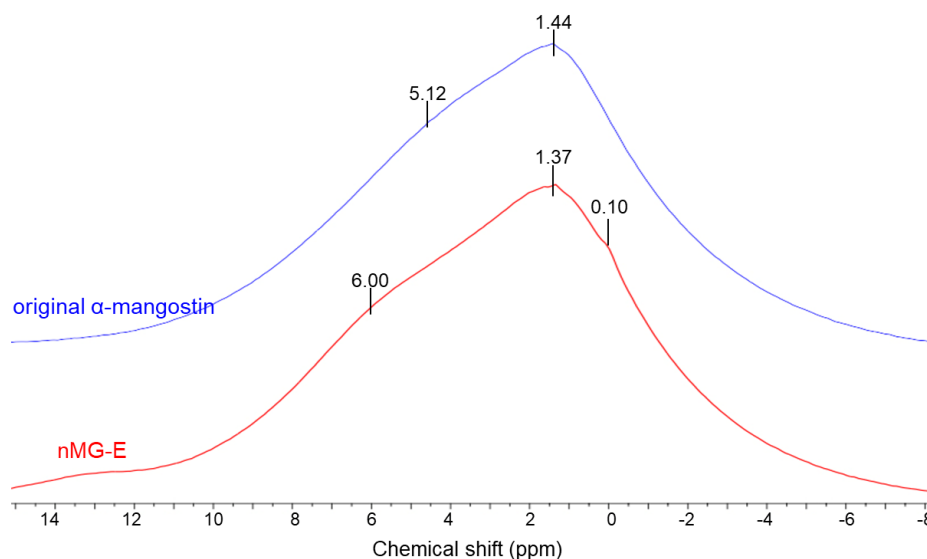


Figure 3.9 Solid-state ^1H NMR spectra of the original α -mangostin solid and nMG-E.

3.2.2 Photophysical property of α -mangostin nanoparticles

UV-Visible spectroscopic analysis was used to study photophysical properties of the materials. The experiments were performed by dissolving original α -mangostin solid, nMG-E, nMG-P and nMG-B in ethanol at 10 ppm. The UV-Visible spectra of the original α -mangostin, nMG-E, nMG-P and nMG-B (Figure 3.10) exhibited the same absorption peak at the maximum wavelength (λ_{max}) of 248 and 321 nm which correspond to $\pi - \pi^*$ transition and $n - \pi^*$ transition, respectively, indicating that the photophysical property in organic solvent of the three particles is the same as that of the original α -mangostin solid. This is not surprising since the measurement was carried out when all materials were in the solution state. As concluded from the liquid state ^1H NMR results that all three materials are actually the same α -mangostin molecules, thus the same UV spectra are not expected.

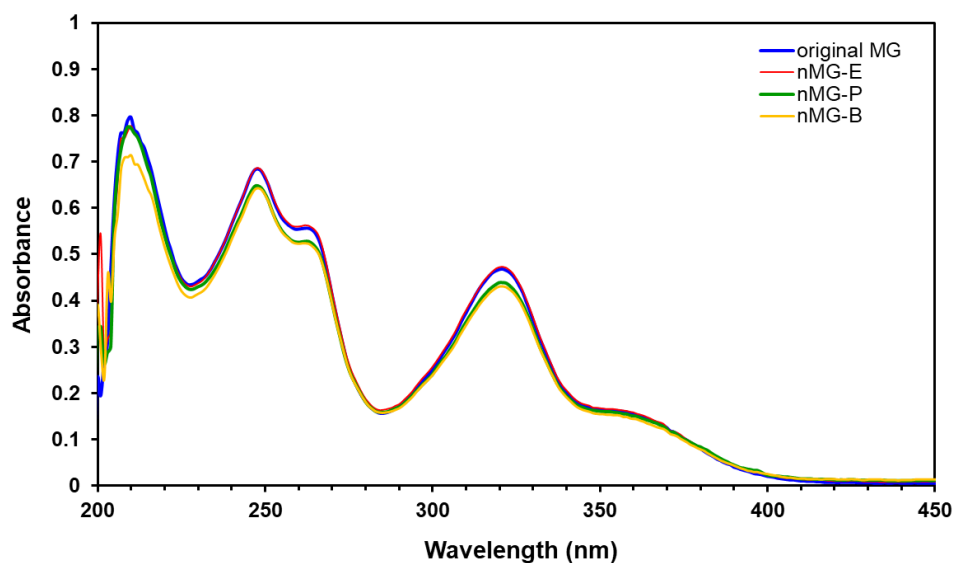


Figure 3.10 UV-Visible spectra of α -mangostin, nMG-E, nMG-P and nMG-B.

3.2.3 Functional group and intermolecular interaction of α -mangostin nanoparticles

FT-IR spectroscopy was used to study the functional group and intermolecular interactions among α -mangostin molecules in the particles. Original α -mangostin solid and the three nanomangostin particles were analyzed at the scanning wavenumber range of 4000 to 500 cm^{-1} .

The FT-IR spectra (Figure 3.11) of the original α -mangostin and the three nanomangostin particles show interesting differences. The O-H stretching vibration of the original α -mangostin appeared as the double broad peaks whereas that of the three α -mangostin particles appeared as a single broad peak, the C-O stretching vibration of vinyl ether of the original α -mangostin appeared as the double peaks whereas that of the three α -mangostin particles appeared as the single peak, and the C-O stretching vibration of C-O connected to hydroxyl group of the original α -mangostin appeared as two sets of the

triple peaks whereas that of the three nanomangostin particles appeared as two sets of the double peaks. These differences suggest that the intermolecular H-bonding involving hydroxyl groups and vinyl ether functional groups of the original α -mangostin solid and of the nanomangostin particles are different.

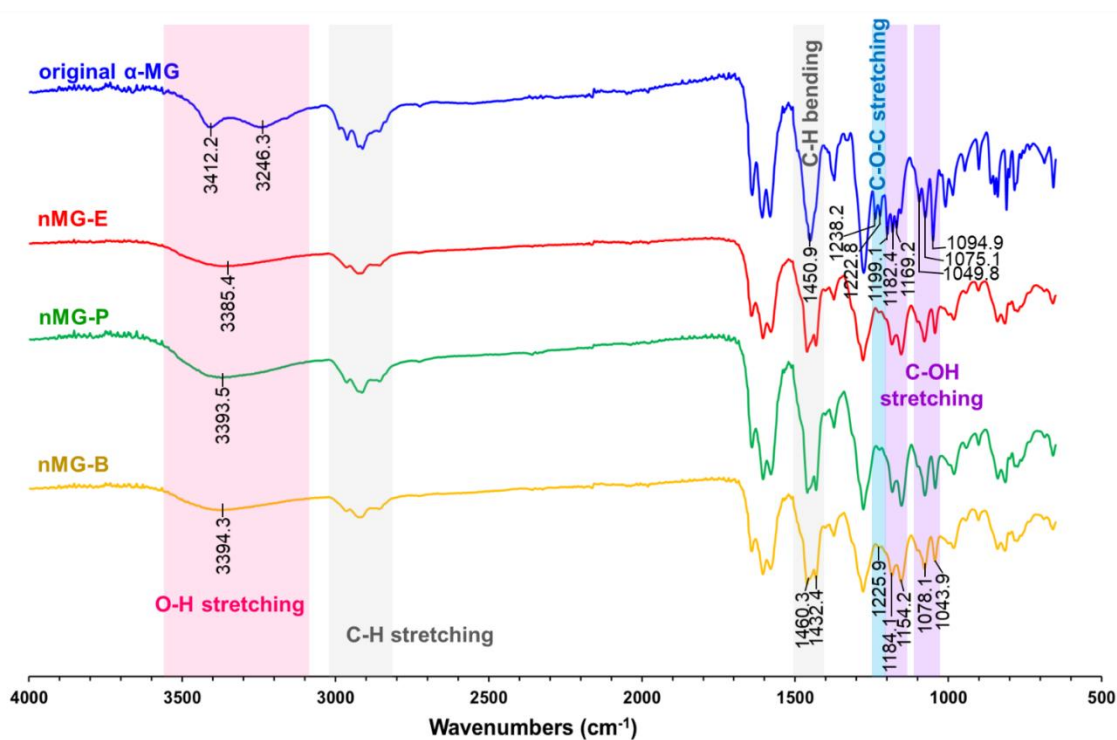


Figure 3.11 IR spectra of the original α -mangostin, nMG-E, nMG-P and nMG-B.

3.2.4 Particle size and zeta potential

Particle size and zeta potential were examined by dynamic light scattering (DLS) at the sample concentration of 0.25 mg/mL in DI water. The hydrodynamic size distribution of nMG-E appears as a gaussian distribution with an average of 370.19 ± 50.00 nm (Figure 3.12). However, the hydrodynamic size distribution of nMG-P is trimodal, i.e., containing a main gaussian at 396 nm and two small distributions at the means of 44 and 106 nm. The size distribution of nMG-B is bimodal, showing two overlapping distribution at the means of 122 and 591 nm (Figure 3.12). Since some molecules of propanol and butanol may be trapped in the particles during the solvent evaporation at the end of the process. We speculated that the bimodal and trimodal distribution arise from the breakup of trapped solvent in particles during the organic solvent evaporation. The average zeta potential of the nMG-E, nMG-P and nMG-B were -34.1 ± 0.72 , -30.1 ± 0.21 and -32.9 ± 1.56 mV, respectively, indicating that all three nanomangostin particles stably disperse in water.

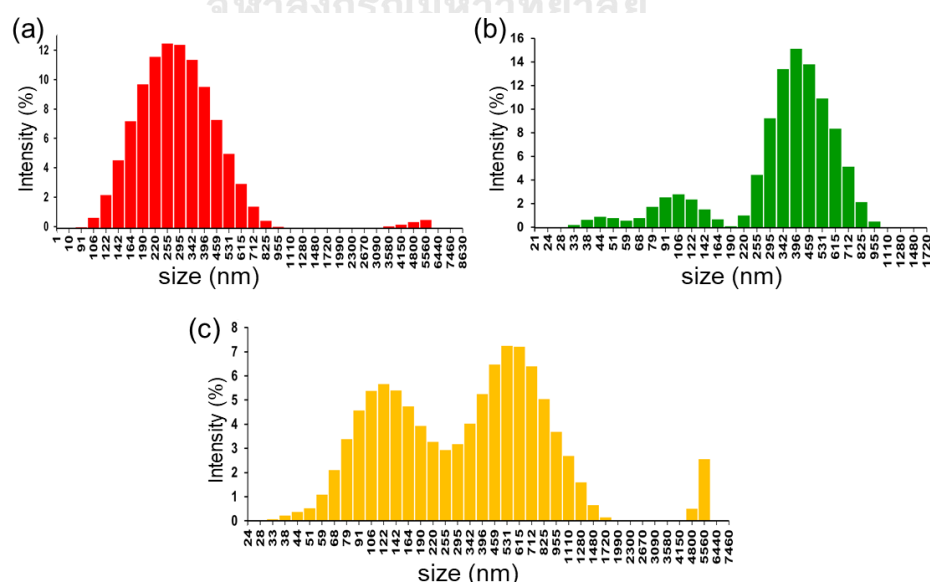


Figure 3.12 Size distribution in water of (a) nMG-E (b) nMG-P and (d) nMG-B.

3.2.5 Crystallinity of α -mangostin nanoparticles

The crystalline character of the original α -mangostin solid, nMG-E, nMG-P and nMG-B were determined using X-ray powder diffraction (XRD) analysis. The XRD pattern of the original α -mangostin (Figure 3.13 blue) indicated crystalline structure with the 2θ at 22.7, 25.6, 26.3, 27.7 and 28.5 which correspond to xanthone skeleton [26], and 16.1, 18.5, 19.2, 20.2, 21.0, 21.8, 23.6, 24.4, 30.8 and 32.6° which probably correspond to xanthone substituents, whereas the XRD patterns of nMG-E, nMG-P and nMG-B (Figure 3.13 red, green and yellow) show a single broad peak. The disappearance of crystallinity implies that the particles is amorphous with less patterned structural packing of α -mangostin molecules as compared to that of the original α -mangostin solid. The result here agrees with the difference in the H-bonding interaction discussed above.

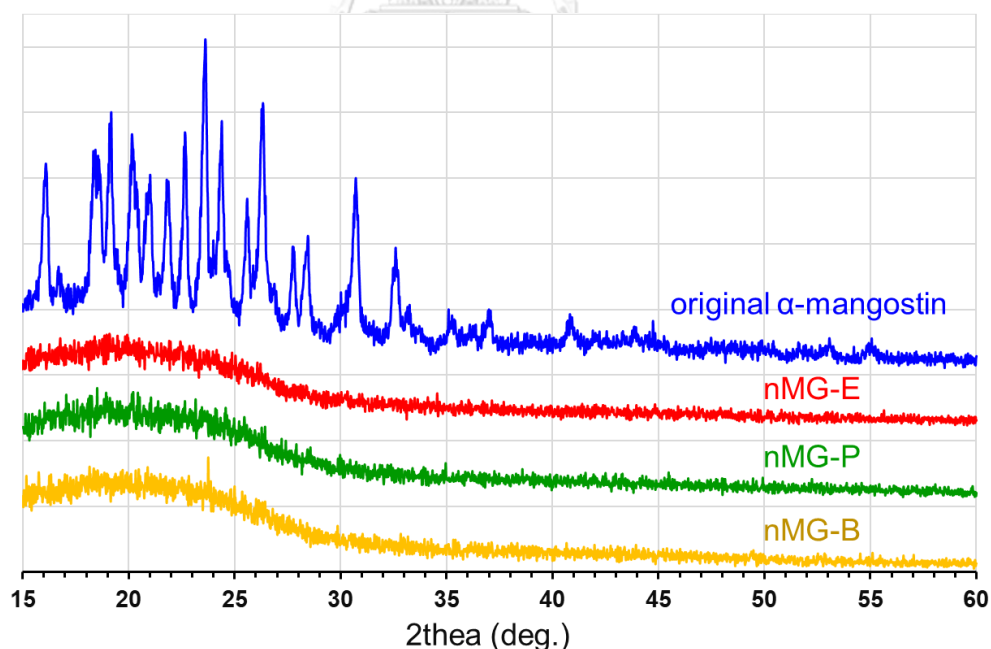


Figure 3.13 X-ray diffraction patterns of the original α -mangostin solid, nMG-E, nMG-P and nMG-B.

3.2.6 Thermal stability of α -mangostin nanoparticles

Thermal stability of the original α -mangostin and nanomangostin particles was determined using thermogravimetric analysis. The thermograms show the maximum decomposition of the original α -mangostin, nMG-E, nMG-P and nMG-B at temperature of 361.62, 347.53, 334.97 and 335.78°C, respectively (Figure 3.14). These results indicate that all three particles are less thermal stable than the original α -mangostin solid. This decreasing thermal stability represents the reduction of strong interaction within particles, which agree with the XRD and FT-IR conclusion above.

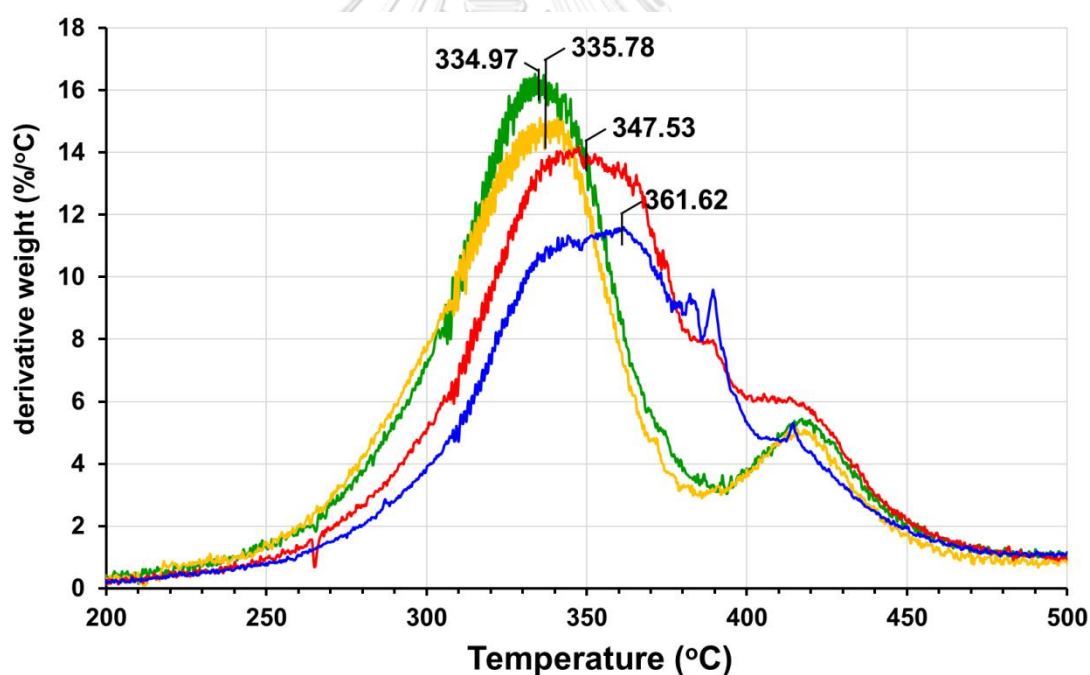
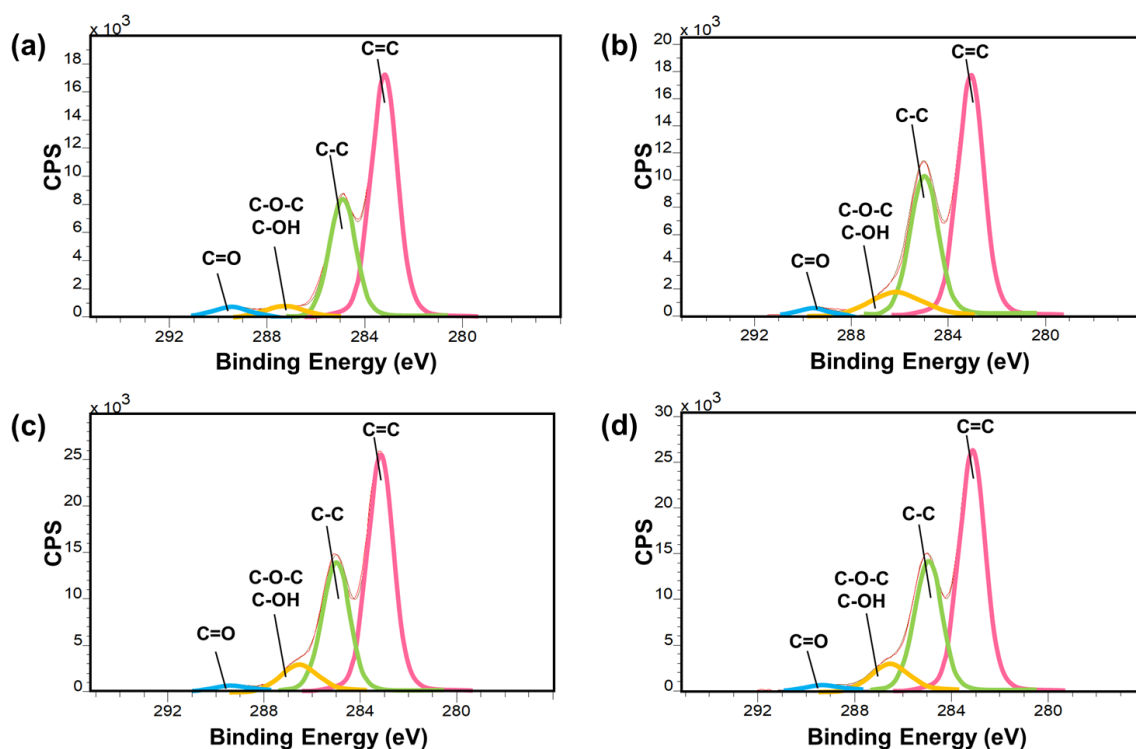


Figure 3.14 Thermograms of the original α -mangostin solid (blue line); nMG-E (red line); nMG-P (green line) and nMG-B (yellow line).

3.2.7 Functional groups at the surface of the particles

The functional groups at the surface of the particles were analyzed by X-ray photoelectron spectroscopy (XPS). The deconvoluted C1s XPS spectra (Figure 3.15) of the three nanomangostin particles show the same deconvoluted peaks to the original α -mangostin solid at the binding energy of 283.2, 285.0, 286.9 and 289.4 eV which correspond to C=C, C-C, C-O-C/C-OH, and C=O bonds, respectively. Likewise, the deconvoluted O1s XPS spectra (Figure A1, Appendix) show the same deconvoluted peaks between the three nanomangostin particles and the original α -mangostin solid at the binding energy of 530.7 and 532.8 eV which correspond to C=O and -OH/O-C-O bonds, respectively. This indicates that all four materials possess the same functional groups. However, the peak area at 286.9 eV (C-O-C and C-OH bond) obviously increased from 4.70% for the original α -mangostin solid to 10.50, 8.66 and 9.14% for the nMG-E, nMG-P and nMG-B, respectively. Because the average depth of analysis for an XPS measurement is approximately 5 nm, the increasing of peak area at C-O-C/C-OH peak indicate that nMG-E, nMG-P and nMG-B particles contained more hydrophilic functional group (C-O-C and C-OH) at their surfaces than the original α -mangostin solid.



	The deconvoluted peak area (%)			
	C=C	C-C	C-O-C and C-OH	C=O
original α -mangostin	57.09	35.58	4.70	2.63
nMG-E	53.62	33.84	10.50	2.04
nMG-P	55.95	33.38	8.66	2.00
nMG-B	55.38	33.49	9.14	1.98

Figure 3.15 XPS results on carbon 1s binding energy of (a) original α -mangostin solid (b) nMG-E (c) nMG-P and (d) nMG-B.

3.2.8 The phenomenon of α -mangostin nanoparticle formation

The above chemical and physical characterization of nanomangostin particles give us the molecular arrangement picture of the nanomangostin particles which is the aggregates of α -mangostin molecules with hydrophilic groups aligned at the surface. We use such information to propose the mechanism of the formation of particles. Before the self-assembly process, the original α -mangostin solid showed the crystalline structure, the molecular packing of the original α -mangostin solid is well-organized with intermolecular H-bonding interaction at the hydroxyl groups and π - π stacking interaction at the aromatic ring system. In the true solution of α -mangostin in ethanol, the original intermolecular interactions among α -mangostin molecules were destroyed. Then, during the water addition into the α -mangostin solution, the solvation of the solvent around each α -mangostin molecule decreased. With more water, the α -mangostin molecules started to aggregate by orienting the hydrophilic groups toward the outer surface to have interaction with water, and xanthone moieties away from water (Figure 3.16). The interaction between hydrophilic groups of α -mangostin and water compensates for the not-well packing of the molecules in the particles. We speculate that the enthalpy compensation from the hydrogen bonding interactions between water molecules and these hydroxyl groups at the particle's surface may be the key driving force that propels the system into the formation of α -mangostin nanoparticles. The obtained α -mangostin nanoparticles can disperse well in water. It is also possible that minute amount of ethanol molecules might be trapped in the particles, but they were all evaporated out during the evaporation process without causing any particle break up as the unimodal size distribution of the particles is observed. In cases of particles made using propanol and

butanol, the size distributions of nMG-P and nMG-B are bimodal and trimodal, respectively. It is likely that with less hydrophobicity of propanol and butanol, comparing to ethanol, more of these solvent molecules were trapped within the particles during the self-assembly of α -mangostin molecules into particles in water-rich medium. We speculated that the trapped propanol and butanol might cause particle break-up during phase separation by solvent evaporation. It should be noted that ethanol (b.p. = 79°C) is more water miscible and evaporate at lower temperature than propanol (b.p. = 97°C) and butanol (b.p. = 117°C).

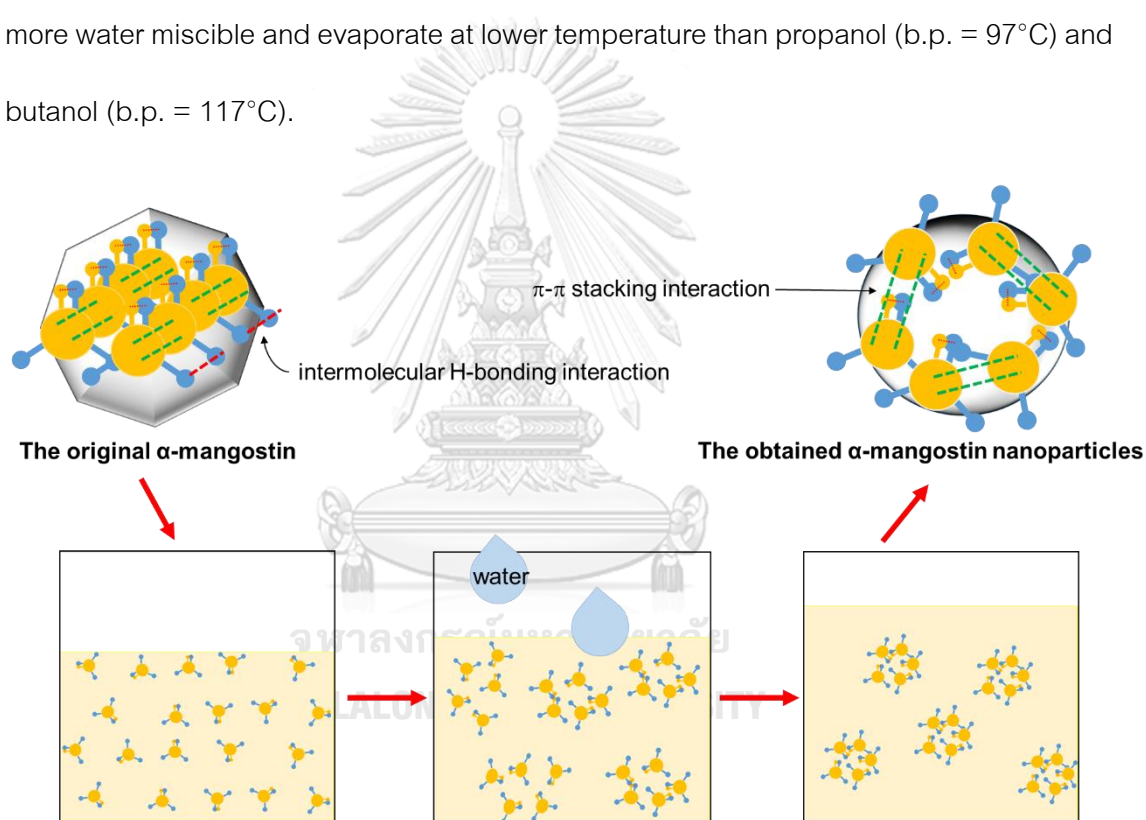
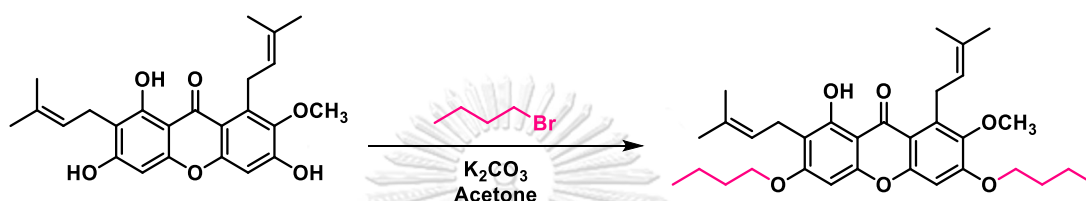


Figure 3.16 The propose schematic represent the phenomenon of α -mangostin nanoparticle formation.

3.3 Self-assembly of α -mangostin derivative

To confirm that the hydroxyl group is essential for α -mangostin particle formation, we synthesize α -mangostin derivative (dMG) by substituting the hydroxyl groups of α -mangostin with butyl groups using S_N2 substitution reaction with bromobutane (scheme 1).



scheme 1. Synthesis of α -mangostin derivative (dMG)

The structure of dibutoxy α -mangostin (dMG) was confirmed by 1H NMR. Bromobutane showed a signal of H_a at 3.42 ppm, but in dMG, the signal is more downfield to 4.05 ppm (Figure 3.17). The integrations of dMG at H_1 : H_4 : H_{11} : H_a : H_c : H_d are 1: 1: 2: 4: 4: 4: 6. These confirm that the two hydroxyl groups of α -mangostin were substituted with two butyl groups.

The obtained dMG was subjected to the same protocol as the preparation of nMG-E particles. The obtained product did not disperse well in water. The SEM image of the product (Figure 3.18) shows the shapeless morphology, indicating that α -mangostin derivative without enough hydroxyl groups could not form water dispersible nanoparticles. These results confirm that the hydroxyl group of α -mangostin molecules is important to form water dispersible α -mangostin particles by the self-assembly process.

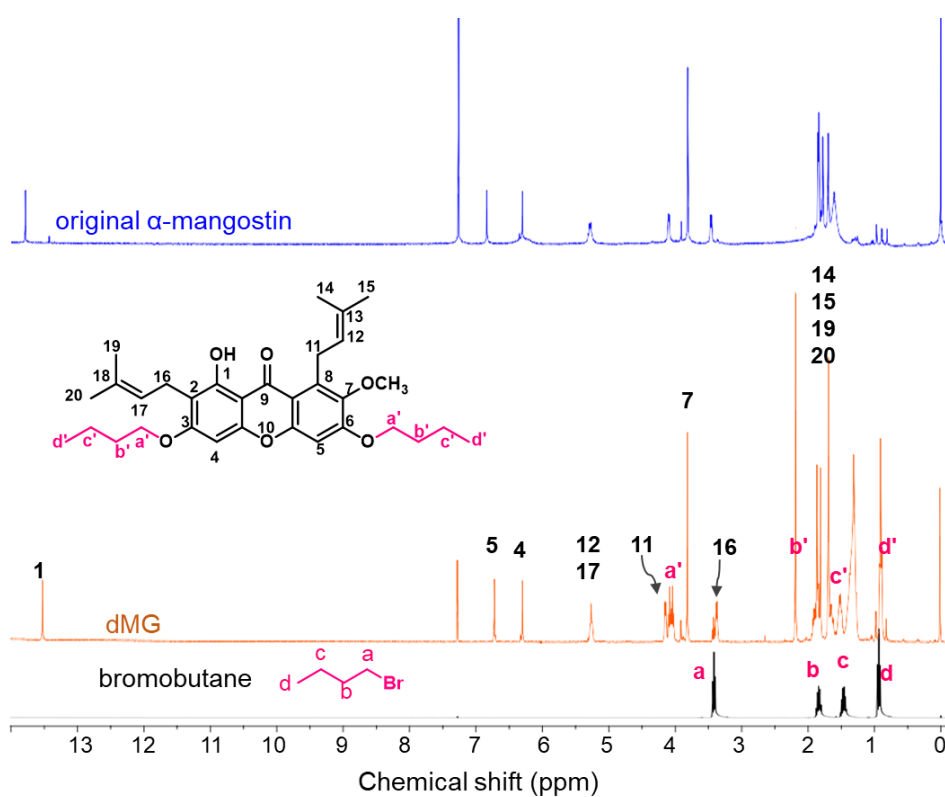


Figure 3.17 NMR spectra of the original α -mangostin solid, dMG and bromobutane.

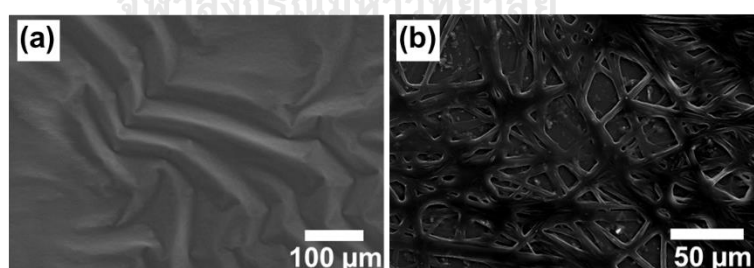


Figure 3.18 SEM images of (a) dMG and (b) the obtained product from self-assembly process of dMG.

3.4 Anti-inflammatory activity and cell viability

Anti-inflammatory activity of the original α -mangostin and nMG-E in water were investigated at the concentrations of 7.12, 9.50, 12.66, 16.88, 22.50 and 30.00 ppm. Anti-inflammatory activity was determined by quantified NO production on RAW 264.7 cell. Cell viability of the tested samples was evaluated using MTT to ensure that the obtained anti-inflammatory activity wasn't due to cytotoxicity effect of α -mangostin.

The anti-inflammatory activities of all tested samples are shown in Figure 3.19. The NO production of the original α -mangostin at concentration of 7.12, 9.50, 12.66, 16.88, 22.50 and 30.00 ppm is 68.75 ± 10.53 , 53.86 ± 6.47 , 51.21 ± 1.42 , 41.19 ± 0.67 , 36.32 ± 1.35 and $23.79 \pm 11.29\%$, respectively. Likewise, the NO production of nMG-E at concentration of 7.12, 9.50, 12.66, 16.88, 22.50 and 30.00 ppm is 27.18 ± 7.77 , 22.61 ± 1.02 , 9.49 ± 2.90 , 7.13 ± 1.02 , 5.37 ± 0.92 and $3.89 \pm 1.55\%$, respectively. The NO production of the two materials decreased as the concentration increased, which indicates that anti-inflammatory activity increased with increasing the concentration of the tested sample. From the %NO production value, anti-inflammatory activity of α -mangostin nanoparticle is significantly higher than that of the original α -mangostin. Thus, it can be concluded that the α -mangostin nanoparticles obtained from self-assembly possess better anti-inflammatory activity than the original α -mangostin. The material is not toxic to the RAW264.7 cells up to 12.7 ppm (>80% cell viability). This discrepancy between the original α -mangostin and the nMG-E may lie at the better cellular uptake of the latter.

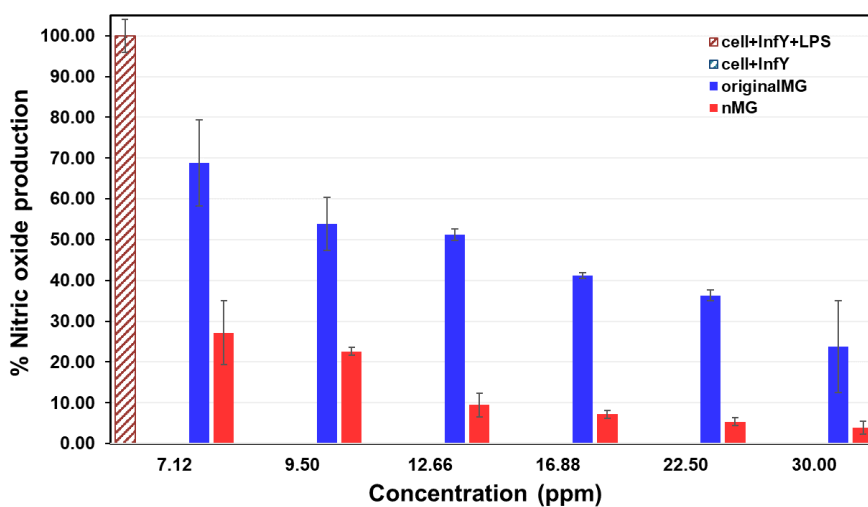


Figure 3.19 %NO production in water of the original α -mangostin solid and nMG-E.

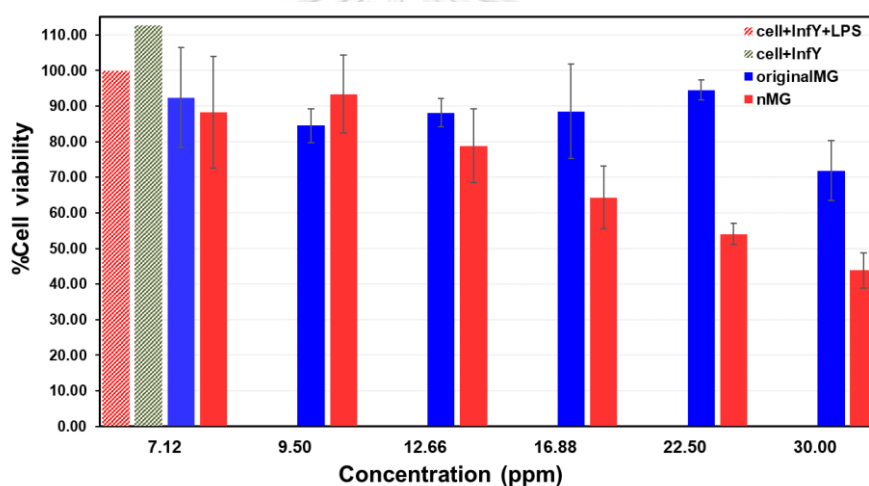


Figure 3.20 %Cell viability in water of the original α -mangostin solid and nMG-E.

3.5 Anti-acne activity

Anti-acne activity of the original α -mangostin solid, nMG-E, nMG-P and nMG-B were investigated at concentration of 1.25, 2.5, 5.0, 10.0 and 20.0 mg/mL using disc diffusion method. We compared the activity of the tested samples by measuring the clear inhibition zone in millimeter (mm). The anti-acne activities of all tested samples are shown in Table 3.1. Clear inhibition zones of the three particles are similar to that of the original

α -mangostin. This result indicates that the water dispersible α -mangostin nanoparticles possess a similar anti *P. acnes* activity comparing to the original α -mangostin solid in 5% v/v DMSO.

Table 3.1 The clear inhibition zone against *P. acne* of the original α -mangostin solid and nanomangostin particles.

Concentration of the tested samples (mg/mL)	Clear inhibition zone (mm)			
	originalMG	nMG-E	nMG-P	nMG-B
1.25	11.83 \pm 0.29	12.33 \pm 0.58	12.17 \pm 0.29	12.17 \pm 0.58
2.5	12.83 \pm 0.29	13.50 \pm 0.50	13.17 \pm 0.29	12.67 \pm 0.58
5.0	14.50 \pm 0.50	15.33 \pm 0.58	15.67 \pm 0.58	15.33 \pm 0.58
10.0	15.17 \pm 0.76	16.50 \pm 0.50	16.50 \pm 0.50	16.33 \pm 0.58
20.0	16.83 \pm 0.29	17.17 \pm 0.29	16.83 \pm 0.29	16.50 \pm 0.50

CHAPTER IV

CONCLUSION

The water dispersible pure α -mangostin had been successfully created from the self-assembly process. The self-assembly process gives 100% pure α -mangostin spherical particles. Investigation revealed that amongst various water miscible organic solvents including dimethyl sulfoxide, methanol, ethanol, propanol, butanol and acetone, only ethanol, propanol and butanol could be used in the process which involved dissolving α -mangostin in organic solvent and slowly introducing water into the system. The three solvents, however, gave particles with small difference in size, e.g. the particle size of nMG-E, nMG-P and nMG-B was 312.17 ± 55.11 , 324.35 ± 71.45 and 467.97 ± 188.51 nm, respectively. Particles from process using the three different solvents also gave particles with high negative surface charge of -34.1 ± 0.72 , -30.1 ± 0.21 and -32.9 ± 1.56 mV for nMG-E, nMG-P and nMG-B, respectively. The ^1H NMR spectra of the nMG-E, nMG-P and nMG-B dissolved into true solution during analysis indicate the same chemical structure as the original α -mangostin. The UV-visible absorption of the three materials in solution state also exhibits the same photophysical property as the original α -mangostin. The solid state ^1H NMR, FT-IR, XRD and TGA results indicate that molecular arrangement, intermolecular H-bonding interactions and molecular packing of the α -mangostin molecules in the particles are different from the original α -mangostin solid. The XPS results indicate that the original α -mangostin solid and three α -mangostin particles possess the same functional groups. But, α -mangostin particles comprised more hydrophilic

functional group at the surfaces than the original α -mangostin solid. These results confirm a new arrangement of α -mangostin molecules into water dispersible particles via our self-assembly process. To clarify the importance of the hydroxyl groups on α -mangostin which are mostly positioned at the surface of the self-assembled particles to the water dispersible character of the prepared particles, we synthesized α -mangostin derivative (dMG) through substitution reaction. The ^1H NMR results of dMG confirm that 3, 6-hydroxyl groups of α -mangostin have been substituted with butyl groups. Next, we prepared water dispersible particles from the obtained dibutoxy α -mangostin using the same protocol as the preparation of the water dispersible α -mangostin particles. Even after various adjustments, water dispersible particles could not be prepared from the obtained dMG. These results indicate that the hydroxyl group on the α -mangostin molecules is important for α -mangostin particle formation. We studied anti-inflammatory activity of α -mangostin particles. The %NO production of the original α -mangostin and α -mangostin particles from the nitric oxide assay indicated that anti-inflammatory activity of α -mangostin nanoparticles was 5 times higher than that of the original α -mangostin at the concentration of 12.7 ppm, which is the concentration that is not toxic to RAW 264.7 cell line. Next, we investigated anti-acne activity of the α -mangostin nanoparticles and comparing to that of the original α -mangostin. We found that the α -mangostin nanoparticles in water can inhibit the growth of *P. acne* similar to the original α -mangostin in 5% DMSO in water. These results indicate that α -mangostin particles obtained from our self-assembly process still possess good biological activities.

REFERENCES

1. Karthiga, P., R. Soranam, and G. Annadurai, Alpha-mangostin, the major compound from *Garcinia mangostana* Linn. Responsible for synthesis of Ag nanoparticles: its characterization and evaluation studies. *Research journal of Nanoscience and Nanotechnology* 2012, 2 (2), 46-57.
2. Doi, H., et al., Panaxanthone isolated from pericarp of *Garcinia mangostana* L. suppresses tumor growth and metastasis of a mouse model of mammary cancer. *Anticancer Research* 2009, 29 (7), 2485-2495.
3. Chen, L.-G., L.-L. Yang, and C.-C. Wang, Anti-inflammatory activity of mangostins from *Garcinia mangostana*. *Food and Chemical Toxicology* 2008, 46 (2), 688-693.
4. Chomnawang, M.T., et al., Antimicrobial effects of Thai medicinal plants against acne-inducing bacteria. *Journal of Ethnopharmacology* 2005, 101 (1-3), 330-333.
5. Jung, H.-A., et al., Antioxidant xanthenes from the pericarp of *Garcinia mangostana* (Mangosteen). *Journal of agricultural and food chemistry* 2006, 54 (6), 2077-2082.
6. Sundaram, B., et al., Antimicrobial activities of *Garcinia mangostana*. *Planta medica* 1983, 48 (05), 59-60.
7. Gopalakrishnan, G., B. Banumathi, and G. Suresh, Evaluation of the antifungal activity of natural xanthenes from *Garcinia mangostana* and their synthetic derivatives. *Journal of natural products* 1997, 60 (5), 519-524.
8. Vlietinck, A., et al., Plant-derived leading compounds for chemotherapy of human immunodeficiency virus (HIV) infection. *Planta medica* 1998, 64 (02), 97-109.
9. Chae, H.-S., et al., Mangosteen xanthenes, α - and γ -mangostins, inhibit allergic mediators in bone marrow-derived mast cell. *Food chemistry* 2012, 134 (1), 397-400.
10. Suksamrarn, S., et al., Antimycobacterial activity of prenylated xanthenes from the fruits of *Garcinia mangostana*. *Chemical and pharmaceutical bulletin* 2003, 51 (7), 857-859.

11. Aisha, A.F., et al., Solid dispersions of α -mangostin improve its aqueous solubility through self-assembly of nanomicelles. *Journal of pharmaceutical sciences* **2012**, *101* (2), 815-825.
12. Lachenmeier, D.W., Safety evaluation of topical applications of ethanol on the skin and inside the oral cavity. *Journal of Occupational Medicine and Toxicology* **2008**, *3* (1), 26.
13. Fei, X., et al., Synthesis of xanthone derivatives based on α -mangostin and their biological evaluation for anti-cancer agents. *Bioorganic & medicinal chemistry letters* **2014**, *24* (9), 2062-2065.
14. Pan-In, P., et al., Depositing α -mangostin nanoparticles to sebaceous gland area for acne treatment. *Journal of pharmacological sciences* **2015**, *129* (4), 226-232.
15. Yang, S., et al., Applying an innovative biodegradable self-assembly nanomicelles to deliver α -mangostin for improving anti-melanoma activity. *Cell death & disease* **2019**, *10* (3), 146.
16. Lademann, J., et al., Nanoparticles—an efficient carrier for drug delivery into the hair follicles. *European Journal of Pharmaceutics and Biopharmaceutics* **2007**, *66* (2), 159-164.
17. Patzelt, A., et al., Selective follicular targeting by modification of the particle sizes. *Journal of controlled release* **2011**, *150* (1), 45-48.
18. Mak, W.C., et al., Triggering of drug release of particles in hair follicles. *Journal of controlled release* **2012**, *160* (3), 509-514.
19. Pukfukdee, P., *Fabrication of particles from tea polyphenol extract for anticancer activity*, in *Department of Chemistry*. 2016, Chulalongkorn University: Bangkok, Thailand.
20. Bumrungpert, A., et al., Xanthenes from mangosteen prevent lipopolysaccharide-mediated inflammation and insulin resistance in primary cultures of human adipocytes. *The Journal of nutrition* **2009**, *139* (6), 1185-1191.

21. Gutierrez-Orozco, F., et al., α -Mangostin: anti-inflammatory activity and metabolism by human cells. *Journal of agricultural and food chemistry* **2013**, *61* (16), 3891-3900.
22. Pothitirat, W., et al., Comparison of bioactive compounds content, free radical scavenging and anti-acne inducing bacteria activities of extracts from the mangosteen fruit rind at two stages of maturity. *Fitoterapia* **2009**, *80* (7), 442-447.
23. Hendra, R., et al., Antioxidant, anti-inflammatory and cytotoxicity of *Phaleria macrocarpa* (Boerl.) Scheff fruit. *BMC complementary and alternative medicine* **2011**, *11* (1), 110.
24. Bernas, T. and J. Dobrucki, Mitochondrial and nonmitochondrial reduction of MTT: Interaction of MTT with TMRE, JC-1, and NAO mitochondrial fluorescent probes. *Cytometry: The Journal of the International Society for Analytical Cytology* **2002**, *47* (4), 236-242.
25. Bonev, B., J. Hooper, and J. Parisot, Principles of assessing bacterial susceptibility to antibiotics using the agar diffusion method. *Journal of antimicrobial chemotherapy* **2008**, *61* (6), 1295-1301.
26. Ho, L.Y., et al., Comparison of physicochemical properties and aqueous solubility of xanthone prepared via oil-in-water emulsion and complex coacervation techniques. *International journal of food properties* **2018**, *21* (1), 784-798.

APPENDIX

1. XPS analysis

1.1 Deconvoluted O1s spectra

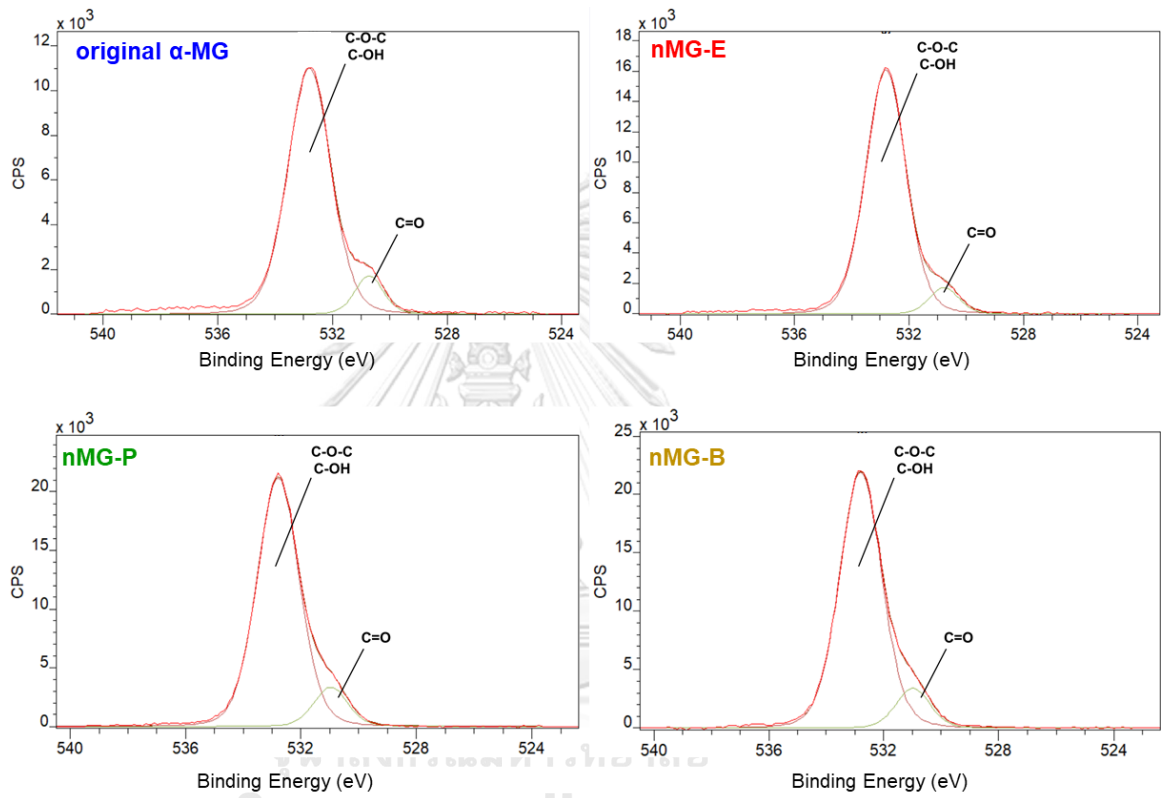


Figure A1. Deconvoluted O1s spectra of the original α -mangostin and nanomangostin particles.

1.2 Calculation of %deconvoluted peak area

The peak area of each functional group was calculated as the percentage of deconvoluted peak area, as follows:

$$\% \text{deconvoluted peak area} = \frac{\text{Deconvoluted peak area}}{\text{Total peak area}} \times 100$$

Table A1. The deconvoluted C1s peak area of the original α -mangostin and nanomangostin particles.

sample	Deconvoluted peak area				Total peak area
	C=C	C-C	C-O-C/C-OH	C=O	
free α -MG	22046.2	13737.9	1814.3	1017	38615.4
nMG-E	24932.3	15734.4	4881.7	946.4	46494.8
nMG-P	34594.4	20641.9	5356.4	1238.7	61831.4
nMG-B	36143.7	21858.2	5965.6	1295.3	65262.8

2. anti-inflammatory activity

2.1 Standard curve of sodium nitrite

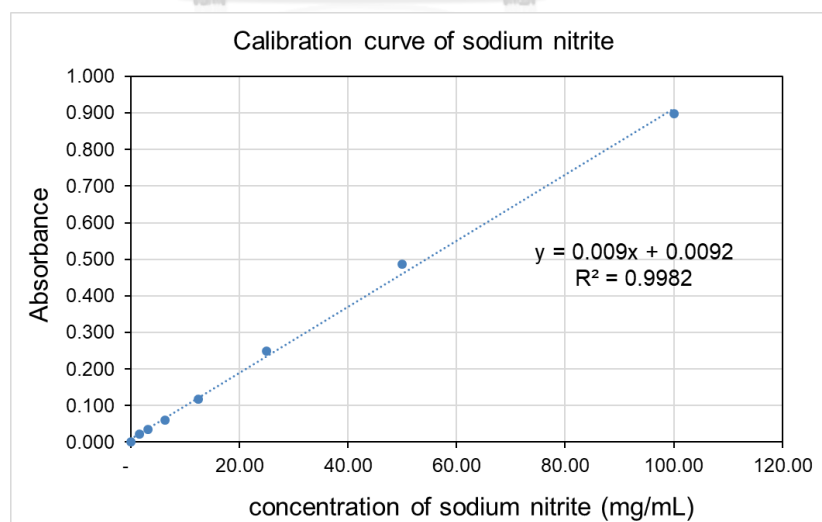


Figure A2. Calibration curve of sodium nitrite.

2.2 Calculation of %NO production

The absorbance obtained from nitric oxide assay (Table A2) was used to quantify nitrite concentration from the equation as follow;

$$y = 0.009x + 0.0092$$

when $y = \text{OD sample} - \text{average OD blank}$

Table A2. The absorbance obtained from nitric oxide assay of the tested samples at 540 nm.

The tested samples	Concentration of the tested samples (mg/mL)	Absorbance		
blank (media)	-	0.079	0.074	0.068
Water + InfY	-	0.084	0.082	0.078
Water + InfY + LPS	-	0.386	0.321	0.334
original MG	7.12	0.255	0.246	0.210
	9.50	0.219	0.19	0.201
	12.66	0.201	0.196	0.195
	16.88	0.176	0.173	0.175
	22.50	0.167	0.163	0.161
	30.00	0.160	0.137	0.109
nMG-E	7.12	0.136	0.13	0.163
	9.50	0.134	0.134	0.13
	12.66	0.097	0.102	0.110
	16.88	0.099	0.095	0.099
	22.50	0.092	0.096	0.093
	30.00	0.087	0.094	0.09

The obtained nitrite concentration of the tested samples was calculated as the percentage of nitric oxide production compared with the nitrite concentration of water, as follows:

$$\%NO \text{ production} = \frac{\text{Nitrite concentration of the tested sample}}{\text{Nitrite concentration of water}} \times 100$$

Table A3. The %NO production of the original α -mangostin and nanomangostin particles.

Concentration of the tested samples (mg/mL)	original MG	nMG-E
7.12	68.75 \pm 10.53	27.18 \pm 7.77
9.50	53.86 \pm 6.47	22.61 \pm 1.02
12.66	51.21 \pm 1.42	9.49 \pm 2.90
16.88	41.19 \pm 0.68	7.13 \pm 1.02
22.50	36.32 \pm 1.35	5.37 \pm 0.92
30.00	23.79 \pm 11.29	3.89 \pm 1.55

3. Calculation of %cell viability

The obtained absorbance obtained from MTT assay (Table A4) was calculated as the percentage of cell viability, as follows:

$$\%Cell \text{ viability} = \frac{OD \text{ sample} - OD \text{ media}}{OD \text{ water} - OD \text{ media}} \times 100$$

Table A4. The absorbance obtained from MTT assay of the tested samples at 540 nm.

The tested samples	Concentration of the tested samples (mg/mL)	Absorbance		
original MG	7.12	0.888	0.766	0.937
	9.50	0.84	0.782	0.821
	12.66	0.808	0.851	0.853
	16.88	0.811	0.774	0.933
	22.50	0.865	0.87	0.897
	30.00	0.766	0.765	0.675
nMG-E	7.12	0.764	0.8	0.95
	9.50	0.791	0.902	0.916
	12.66	0.714	0.78	0.843
	16.88	0.642	0.672	0.749
	22.50	0.603	0.629	0.639
	30.00	0.554	0.593	0.532

Table A5. The % cell viability of the original α -mangostin and nanomangostin particles.

Concentration of the tested samples (mg/mL)	original MG	nMG-E
7.12	92.37 \pm 14.05	88.27 \pm 15.74
9.50	84.50 \pm 4.72	93.33 \pm 10.93
12.66	88.17 \pm 4.06	78.86 \pm 10.29
16.88	88.49 \pm 13.27	64.29 \pm 8.81
22.50	94.56 \pm 2.75	54.08 \pm 2.96
30.00	71.90 \pm 8.34	43.87 \pm 4.93

4. anti-acne activity

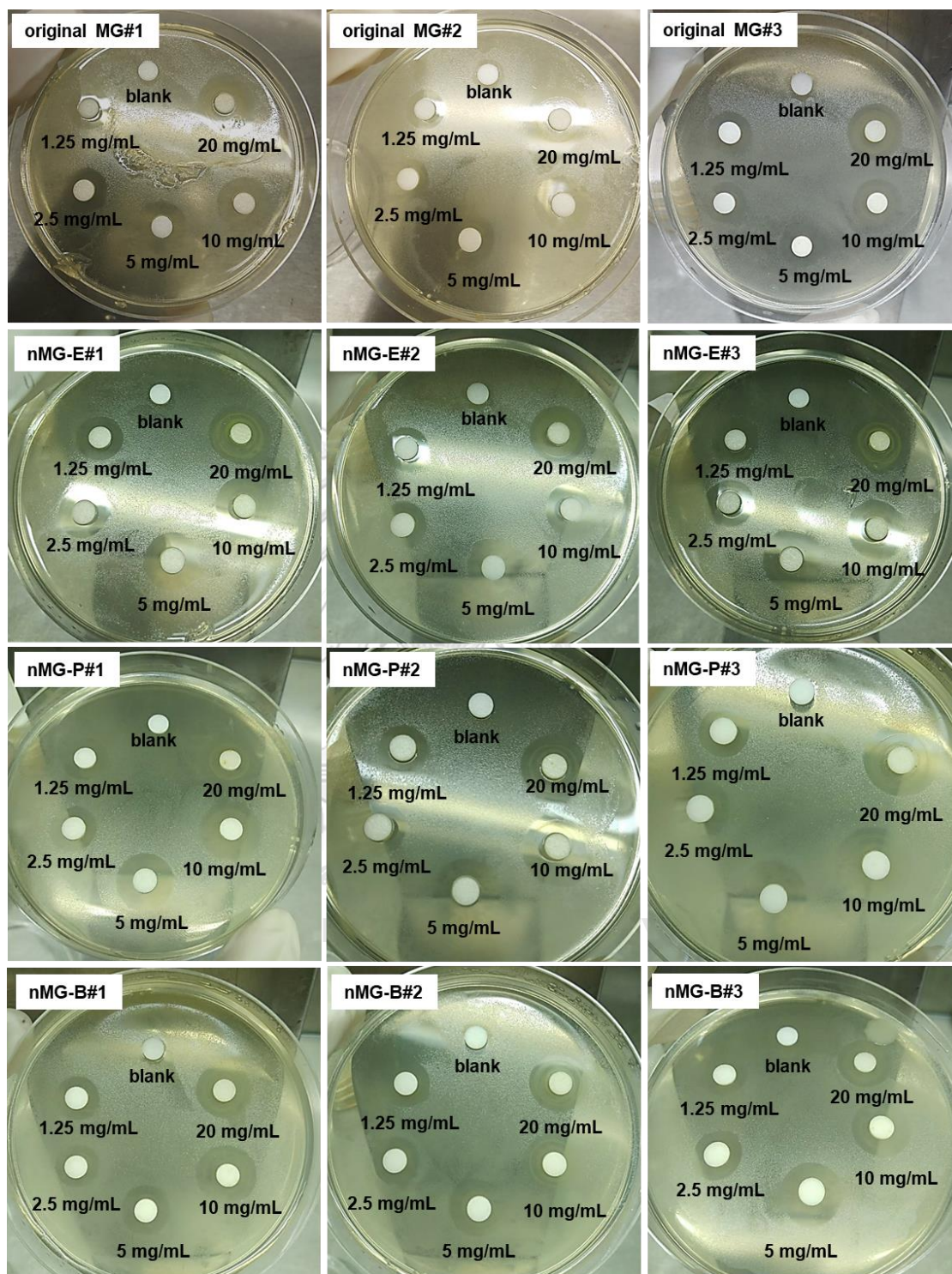


Figure A3. The clear inhibition zone against *P. acne* of the original α -mangostin and nanomangostin particles.

VITA

NAME Jutamad Bumrung

DATE OF BIRTH 27 February 1995

PLACE OF BIRTH Suratthani

INSTITUTIONS ATTENDED Bacher's degree of science from Department of Chemistry,
Faculty of Science, Silpakorn University, Nakornpathom
Thailand in 2017.

HOME ADDRESS 36 Village No.1, Phunphin, Suratthani 84130

